Biophysical variability at the shelf-break/slope transition: Insights from a high-resolution transect experiment in the Southwestern Tropical Atlantic

Syumara Queiroz, Ramilla Vieira de Assunção, Leandro Nolé Eduardo, Alex Costa da Silva , Moacyr Araujo , Arnaud Bertrand

https://doi.org/10.1590/SciELOPreprints.17079

Submitted on: 2026-07-23
Posted on: 2026-07-23 (version 1)
(YYYY-MM-DD)

Multiple Rectangles Transect experiment

Biophysical variability at the shelf-break/slope transition: Insights from a high-resolution transect experiment in the Southwestern Tropical Atlantic

Syumara Queiroz [1,2*], Ramilla Vieira de Assunção [1,2], Leandro Nolé Eduardo[2,3], Alex Costa da Silva [1,2], Moacyr Araujo [1,2,4], Arnaud Bertrand [2,3]

S.Q.: https://orcid.org/0000-0002-9408-8693
R.V.A.: https://orcid.org/0000-0001-5495-6858
L.N.E.: https://orcid.org/0000-0003-2369-4175
A.C.S.: https://orcid.org/0000-0002-5828-3598
M.A.: https://orcid.org/0000-0001-8462-6446
A.B.: https://orcid.org/0000-0003-4723-179X

1 Laboratory of Estuarine and Coastal Physical Oceanography (LOFEC), Department of Oceanography, Federal University of Pernambuco, Av. Arquitetura, 50740-550, Recife, Pernambuco, Brazil.
2 IJL TAPIOCA: International Joint Laboratory - Tropical Atlantic Interdisciplinary laboratory on physical, biogeochemical, ecological and human dynamics. Federal University of Pernambuco, Av. Arquitetura, 50740-550, Recife, Pernambuco, Brazil.
3 Institut de Recherche pour le Développement (IRD), MARBEC (Univ Montpellier, CNRS, Ifremer, IRD), 34203 Sète, France.
4 Brazilian Research Network on Global Climate Change – Rede CLIMA, 12227-010, São José dos Campos, São Paulo, Brazil.
* Corresponding author: syumaraqueiroz@hotmail.com

ABSTRACT

We investigated how short-term physical variability influences biological distributions at the shelf-break and slope off Northeast Brazil using a process-oriented Multiple Rectangle Transect (~2 × 11 km) repeated over ~26 h, spanning two semidiurnal tides and a full diel cycle. Co-located measurements combined ship-mounted acoustic Doppler current profiling, multifrequency echosounders (38, 70, 120 kHz), continuous thermosalinograph data, and targeted CTD/XBT profiles. Shallow (15–59 m) along- and cross-shelf current series were analyzed with Ensemble Empirical Mode Decomposition to isolate dominant variability scales, and barotropic tidal constituents from a global model were used for comparison. The velocity structure was dominated by the North Brazil Undercurrent, with a jet core (~70–350 m) peaking at 0.6–0.8 m s^{-1} and a weakened layer around 160–230 m within the core. Near-surface along-shelf flow remained positive (mean ~0.35 m s^{-1}), while cross-shelf flow alternated between shoreward and seaward. Semidiurnal tides explained most shallow variability and organized alternating convergence-divergence patterns across the rectangle; observed amplitudes exceeded tidal model estimates, indicating interaction with the background current. Hydrography showed a warm mixed layer over a sharp thermocline, with a subsurface chlorophyll maximum (~90–110 m) and cooler, oxygen-reduced layers below the undercurrent core. Acoustic data revealed diel vertical migration and multiple sound-scattering layers (SSLs). During daytime, key SSLs preferentially occupied reduced-velocity zones (~100 m above the current maximum and ~205 m within the weakened layer), indicating that fine-scale current structure influenced their vertical organization. The recurrent association of the ~205 m aggregation with the weakened layer suggests that such low-velocity zones may provide favorable conditions for vertically migrating organisms. Deeper SSLs (~310–400 m) coincided with reduced currents

and lower oxygen. Overall, the results suggest that flow–topography interactions at the slope create localized low-velocity structures that influence mesopelagic distributions on submesoscales.

KEYWORDS: BIOPHYSICAL INTERACTIONS, FLOW-TOPOGRAPHY INTERACTIONS, DIEL VERTICAL MIGRATION, WESTERN BOUNDARY CURRENT, SOUTHWESTERN TROPICAL ATLANTIC

INTRODUCTION

Continental shelf-break and slope (hereafter SBS) mark the transition between shallow continental shelves and the deep ocean, where processes occurring across a broad range of spatial (meters to tens of kilometers) and temporal scales (hours to months) interact, modulating biological productivity and ocean-atmosphere exchanges (Huthnance, 1995; Acha et al., 2004; Genin, 2004). These zones are dynamically complex, with strong physical gradients and energetic processes such as fronts, eddies, internal waves, and tides, which together drive exchanges of heat, momentum, nutrients, and biota between coastal and oceanic domains (Brink, 2016). Interactions between boundary currents and topography can generate substantial cross-shelf transport, alter water-mass characteristics, and create localized biological hotspots (Oke and Middleton, 2000; Roughan and Middleton, 2002; Castelao, 2011).

The high variability and fine spatial and temporal scales of SBS dynamics make them challenging to study. Traditional oceanographic sampling methods, such as sparse hydrographic sections or low-frequency remote sensing products, often fail to capture the short-lived, small-scale features that structure these environments (Brink, 2016; Lévy et al., 2018). As a result, direct in situ observations with adequate spatial and temporal resolution are scarce, particularly in oligotrophic tropical western boundary current systems, where logistical and operational constraints limit sustained measurements.

In the Southwestern Tropical Atlantic (SWTA), the SBS off Northeast Brazil is influenced by the North Brazil Undercurrent (NBUC; Fig. 1a), a strong subsurface western boundary current that flows equatorward from the bifurcation of the southern branch of the South Equatorial Current (sSEC) (Stramma et al., 1995; Schott et al., 2002, 2005; Silva et al., 2009a, 2009b; Dossa et al., 2021a). The NBUC plays a major role in the inter-hemispheric heat transport as part of the Atlantic Meridional Overturning Circulation (AMOC), and its interaction with the Pernambuco Plateau and other topographic features can generate complex circulation patterns and vertical motions near the shelf break (Silva et al., 2022), including persistent shelf-ward flows that were reported (Domingues et al., 2017) but not fully investigated. Furthermore, despite the importance of this region, in situ datasets resolving the SBS dynamics are rare, and even fewer include simultaneous high-resolution measurements of both physical and biological variables.

Biological structuring in SBS regions is often mediated by fine-scale hydrodynamic processes. Physical gradients, such as those generated by boundary currents, can aggregate plankton and micronekton, influence diel vertical migration, and modulate predator-prey interactions (Genin et al., 2005; Bertrand et al., 2014; Sato and Benoit-Bird, 2024). In the SWTA, however, the coupling between physical and biological processes at the SBS has been poorly documented, largely due to the absence of coordinated multidisciplinary observations at adequate scales. While large-scale patterns in this region were documented by the REVIZEE program (Weigert and Madureira, 2011), fine-scale processes have only recently been investigated through the Acoustics along the Brazilian Coast 1 and 2 (ABRAÇOS 1, Bertrand, 2015; ABRAÇOS 2, Bertrand, 2017) projects, particularly in Assunção et al. (2023).

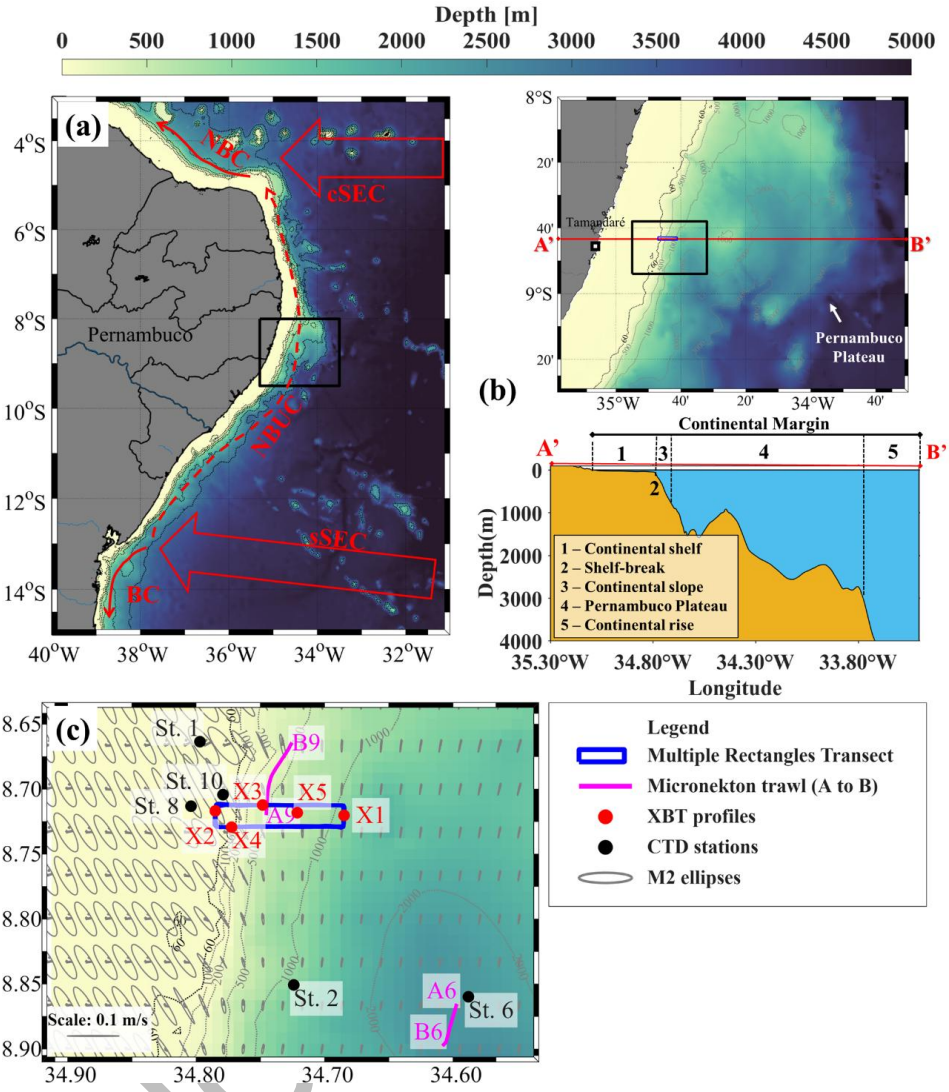

Figure 1. Study region and experimental design in the Southwestern Tropical Atlantic. (a) Regional circulation off Northeast Brazil, showing the main surface and subsurface currents. Broad red arrows indicate the central and southern branches of the South Equatorial Current (cSEC and sSEC), with the mean sSEC bifurcation near 13°S. Narrow red arrows show the surface North Brazil Current (NBC) and Brazil Current (BC), and the dashed red arrow indicates the subsurface North Brazil Undercurrent (NBUC). The black square marks the area enlarged in panel (b). (b) Upper panel: zoom of the southern Pernambuco continental margin and Pernambuco Plateau. The black rectangle marks the Multiple Rectangles Transect (MRT) region shown in panel (c), and the red A′–B′ line indicates the bathymetric cross-section. Lower panel: bathymetric section along A′–B′ at 8.7229°S, showing the continental shelf (1), shelf break at ~60 m depth (2), continental slope (3), Pernambuco Plateau between the 700 and 3000 m isobaths (4), and continental rise toward the deep ocean (5). (c) Detailed view of the MRT region. The blue outline shows the approximately 2 by 11 km MRT box. Black circles indicate conductivity–temperature–depth stations, red circles indicate expendable bathythermograph drop points, and dotted contours show GEBCO bathymetric isobaths at 30″ resolution (Weatherall et al., 2015). Magenta lines show pelagic micronekton trawls conducted before (A6–B6) and after (A9–B9) the MRT experiment. M2 tidal ellipses from TPXO9 (gray) indicate the orientation and magnitude of barotropic tidal currents; ellipse scale corresponds to 0.1 m s^{-1}.

Using multi-frequency acoustics, hydrography, and ship-mounted Acoustic Doppler Current Profiler

(SADCP)-derived currents, Assunção et al. (2023) provided important insights into diel vertical migration and its environmental drivers across stations located on and near the slope. However, despite these contributions, the station-based approach, which averaged current measurements over a fixed radius around CTD locations, does not capture the continuous spatial and temporal variability of currents and biological layers along the shelf–slope transition. Furthermore, their sampling emphasized deeper slope stations (>300 m), leaving the immediate shelf-break zone less represented. Relationships between biology and physics were evaluated at discrete points, limiting the ability to detect transient or fine-scale features.

Our study complements the work by Assunção et al. (2023) through a process-oriented experiment executed in April of 2017, during the ABRAÇOS 2 survey (Bertrand, 2017). The Multiple Rectangle Transect (MRT) experiment consists of repeating transects around a predefined rectangular path enabling quasi-synoptic sampling of spatial and temporal variability at submesoscale resolution (Bertrand et al., 2008a). In this study, the MRT was specifically designed sample across the shelf-break and slope throughout an entire diel cycle, providing continuous, co-located measurements cross- and along-shelf sections of current velocity profiles and multifrequency acoustic backscatter from biological sound-scattering layers (SSLs). Using this unique dataset, we aimed to characterize the short-scale physical variability across the shelf-break and slope under the influence of the North Brazil Undercurrent and to test whether fine-scale current structures, including reduced-velocity zones within the current core, were associated with the diel distribution and vertical organization of biological layers observed by multifrequency acoustics.

METHODS

STUDY AREA AND SURVEY DESIGN

The experiment was conducted over the northeastern Brazilian continental shelf-break and adjacent slope (Fig. 1a) between 9 and 12 April 2017, during the Acoustics along the BRAzilian COaSt 2 (ABRAÇOS 2) survey aboard the R/V Antea (Bertrand, 2017). The study region is located in the SWTA, where the shelf-break is ~60 m deep (Camargo et al., 2007), the continental slope extends to the Pernambuco Plateau (~700 m; Fig. 1b) (Zembruscki et al., 1972; Coutinho, 1996), and the subsurface circulation is dominated by the northward-flowing NBUC (Schott et al., 2002, 2005; Hummels et al., 2015; Dossa et al., 2021a).

The MRT experiment was performed to resolve the spatial-temporal variability of physical and biological conditions at submesoscale resolution. The MRT consisted of repeated transects around a fixed 2 km × 11 km rectangular path positioned across the shelf-break (8.711°S – 8.730°S, 34.785°W – 34.684°W) (Fig. 1c) for ~26 hours (from 11 April 19:17 to 12 April 20:45 UTC), covering two semidiurnal spring-tide cycles and a complete diel cycle. Each rectangle transect required ~1 h 45 min to be completed, resulting in 15 full repetitions.

This sampling design provided near-synoptic horizontal coverage while allowing for the detection of small-scale temporal variability and diel vertical migrations. All acoustic and physical sensors were operated continuously throughout the experiment, and hydrographic profiles were collected before, during, and after the MRT to characterize the thermohaline structure.

PHYSICAL MEASUREMENTS

Current velocities were measured using a Ocean Surveyor SADCP (75 kHz). In deep water (>150 m bottom depth), data were acquired every 3 s with an 8 m vertical bin; in shallow water (<150 m), data were

acquired every 1 s with a 4 m vertical bin. Horizontal meridional (V) and zonal (U) components from each ping were vector-averaged into 2-min ensembles using VmDAS software, quality-controlled, and converted to netCDF format with CASCADE tools (Herbert et al., 2015).

To investigate spatial patterns relative to topography, V and U were rotated into along-shelf (AS) and cross-shelf (CS) components using the local slope orientation derived from high-resolution bathymetry from a hull-mounted echosounder Simrad EK60. For the rotation, we applied the system of equations below given by Brink (2016), where θ is the angle in relation to the meridional direction (mean/max θ = 0.39°/1.0732°).

$$\begin{cases} CS = U\ cos\,\theta + V\ sin\,\theta \\ AS = -U\ sin\,\theta + V\ cos\,\theta \end{cases}$$

Furthermore, currents were not de-tided; instead, tidal currents were estimated from the TPXO9-atlas barotropic tidal model (Egbert and Erofeeva, 2002; Erofeeva, 2022) for direct comparison. The same rotation procedure presented above was used to rotate modelled semidiurnal components (M2, S2, K2, N2) named AS-TIDE, and CS-TIDE for the same coordinates and times of the MRT.

Sea surface temperature (SST) and salinity (SSS) were recorded continuously with a thermosalinograph composed of a SEABIRD SBE38 thermometer and an SBE21 conductivity sensor. Vertical profiles of temperature, salinity, dissolved oxygen, and chlorophyll-a fluorescence were collected with a rosette-mounted SeaBird SBE911+ CTD equipped with a Wetlabs® ECO fluorometer at selected stations before and after the MRT. Additional temperature profiles were obtained with Sippican T-10 expendable bathythermographs (XBTs) during and after the MRT (Table 1).

Table 1. Latitude and Longitude (in decimal degrees), date and time for selected Conductivity-Temperature-Depth (CTD) profiles (denoted by 'ST') and Expendable Bathythermograph (XBT) profiles (denoted by 'XBT') collected during the ABRAÇOS 2 survey.

Profile	Latitude	Longitude	Date Time
ST1	8.6635°S	34.797°W	09-Apr-2017 16:35:35
ST2	8.8506°S	34.724°W	09-Apr-2017 20:44:18
ST6	8.8597°S	34.588°W	11-Apr-2017 09:57:02
ST8	8.7131°S	34.804°W	11-Apr-2017 18:45:21
ST10	8.7043°S	34.779°W	13-Apr-2017 01:16:36
XBT1	8.7201°S	34.6848°W	11-Apr-2017 23:16:00
XBT2	8.7168°S	34.7851°W	12-Apr-2017 00:09:00
XBT3	8.7123°S	34.7481°W	12-Apr-2017 00:27:00
XBT4	8.7292°S	34.7723°W	12-Apr-2017 01:41:00
XBT5	8.7181°S	34.7212°W	12-Apr-2017 21:10:00

Furthermore, as ancillary data, we used Copernicus Marine Service reanalysis products to provide broader regional context for the in-situ observations. Hourly wind reanalysis fields were examined to characterize the regional wind conditions during the survey, using averages over a window bounded by 34.9375°W–34.5625°W and 8.9375°S–8.6875°S. In addition, monthly fields from the Global Ocean Physics Reanalysis - GLORYS (1993–2016) were used to investigate whether the weakened NBUC core observed during the MRT could also be inferred at broader spatial and temporal scales in nearby transects at 9.25°S, 8.75°S, and 8.25°S. These ancillary products were not used to resolve the fine-scale processes sampled by

the MRT, but rather to place the local observations in a broader atmospheric and oceanographic context.

SHALLOW CROSS-SHELF AND ALONG-SHELF CURRENT VARIABILITY

Since the higher current variability was observed at depths shallower than the shelf-break, we applied Ensemble Empirical Mode Decomposition (EEMD; Wu and Huang, 2009) to the shallow current records, averaged between 15 and 59 m, for the along- and cross-shelf components (hereafter ASavg and CSavg), with the specific aim of identifying the dominant scales of variability. This adaptive decomposition separates each signal into Intrinsic Mode Functions (IMFs), which isolate variability at distinct characteristic scales without prescribing a priori basis functions (Wu and Huang, 2009). The IMFs were obtained using the Python EEMD module of the PyEMD package (https://github.com/laszukdawid/PyEMD).

Because the Multiple Rectangle Transect (MRT) is a repeated mobile survey rather than a fully synoptic occupation, the decomposed record must be interpreted as a mixed spatiotemporal signal rather than as a purely Eulerian time series. In this context, part of the variance captured by a given IMF may reflect temporal variability, whereas part may arise from the repeated crossing of persistent spatial gradients and topographic features, particularly at scales comparable to the MRT repetition time and its harmonics. This limitation is consistent with previous work showing that uneven sampling in both space and time complicates the processing of SADCP records and may introduce space-time aliasing or spurious tidal constituents if not carefully interpreted (Chiao and Wang, 2004). For this reason, in our case the physical meaning of the retained IMFs was assessed jointly with the ship trajectory, the bathymetry, and the independent tidal-model results. Only IMFs explaining more than 5% of the total variance were retained to focus the analysis on physically relevant modes. In practice, some modes represented the dominant cross-shore gradient between the shelf and oceanic sides of the transect, whereas others capture variability localized near the shelf-break. Similar adaptive decomposition approaches have been successfully applied to other geophysical observations obtained along moving tracks, including seismic sections, for which EEMD was shown to reduce scale-mixing problems relative to conventional EMD (Song et al., 2012), and along-track altimetry, for which Hilbert–Huang or EMD-based methods have been used to extract frontal or current-related variability from nonlinear, nonstationary records while preserving strong spatial gradients (Dong et al., 2018; Quilfen and Chapron, 2019, 2021).

Hilbert Transform was then applied to the selected IMFs to determine instantaneous amplitudes and frequencies (Wu and Huang, 2009), allowing us to evaluate how the strength and characteristic timescales of these gradients evolved during the MRT experiment. This leads to the Hilbert spectrum, which offers results comparable to the wavelet magnitude scalogram for energy-frequency distributions, but with improved temporal and frequency resolution, making it particularly effective for identifying transient and nonlinear features in oceanographic data (Huang and Shen, 2014; Kbaier et al., 2016).

BIOLOGICAL BACKSCATTER

Biological backscatter was measured continuously with a hull-mounted Simrad EK60 scientific echosounder operating at 38, 70, and 120 kHz. The system was calibrated before the survey following standard protocols, and acquisition parameters were adjusted to bottom depth: for depths <150 m, the ping interval was 0.45 s, and for depths up to 750 m, the ping interval was 2.4 s. The EK60 was synchronized with the SADCP to ensure co-located biological and physical measurements. Acoustic data was processed using Echoview® software. Echointegration was performed at a horizontal resolution of 1 ping and vertical resolution of 0.5 m, from 15 to 500 m depth. Backscatter strength (Sv, dB re 1 m^{-1}) was obtained with a threshold between -50 and -100 dB (following Assunção et al., 2023).

To visualize frequency-specific scattering, Red-Green-Blue (RGB) echograms were generated by assigning 38 kHz to red, 70 kHz to green, and 120 kHz to blue channels (Ariza et al., 2023; Assunção et al., 2023). Mixed or frequency-dominant targets appeared as composite or single-color signals, respectively. Acoustic SSLs were identified in echograms and compared with coincident physical measurements (currents, hydrography) to assess associations between biological distributions, hydrodynamic structures, and diel vertical migration patterns. Particular attention was given to the occurrence of SSLs in regions of reduced current velocity detected within the MRT domain.

PELAGIC MICRONEKTON TRAWLS

To provide biological support for the interpretation of acoustically similar fish-like layers, we recovered the taxonomic data from two targeted pelagic micronekton trawls conducted during the ABRAÇOS 2 survey. These trawls were performed along transects A6–B6 and A9–B9 (Fig. 1), outside but close in time to the MRT experiment, and targeted discrete acoustic layers identified in the RGB echograms. In both cases, the same pelagic trawl was used, with a mouth opening of 24 × 24 m, a body mesh size of 40 mm, and a cod-end mesh size of 10 mm. One tow started at 11:24 on 11 April 2017 (A6-B6) and sampled echoes between 240 and 260 m for approximately 30 min, whereas the second tow started at 21:51 on 12 April 2017 (A9-B9) and sampled echoes between 85 and 135 m for approximately 35 min. Detailed information on specimen identification and the taxonomic treatment of the sampled material is available in Eduardo et al. (2020; 2021).

RESULTS

GENERAL PATTERNS AND VARIABILITY DURING THE EXPERIMENT

Winds remained weak throughout the MRT experiment (11–12 April), averaging 2.05 ± 0.80 m s^{-1} with a persistent E–SE quadrant, and did not exhibit energetic bursts capable of directly driving surface currents (Fig. 2a). Along the ship track, the sampled bottom depth varied widely as the section crossed the upper slope repeatedly, consistent with the repeating pattern of the transects (Fig. 2b). Surface hydrography was likewise steady: SSS was 37.41 ± 0.07 with a total excursion of 0.25, and SST was 28.90 ± 0.18 °C with an excursion of 0.73 °C (Figs. 2c-d).

The velocity field exhibited a classic NBUC structure (Figs. 2e-f). Absolute speed was modest in the upper 50–70 m (~0.35 m s^{-1}) and intensified beneath, reaching ~0.6 m s^{-1} within the jet core that occupied roughly 70–350 m (Fig. 2e). Following Dossa et al. (2021), we defined the core as speeds ≥70% of the maximum along-shelf flow; with a local maximum of ~0.78 m s^{-1}, the core threshold was >0.55 m s^{-1}. The core was not vertically uniform: a weaker interleaving layer near ~160–230 m intermittently reduced speeds below the 0.55 m s^{-1} threshold, splitting the core into upper and lower jets. Beneath ~350 m, velocities decayed from ~0.6 to ~0.45 m s^{-1} toward 500 m.

Depth-mean profiles confirmed a strongly along-shelf-dominated flow with small cross-shelf shear (Fig. 2f). Time series of layer-averaged currents (15–59 m) showed that the along-shelf component stayed positive throughout (mean = 0.35 ± 0.08 m s^{-1}; range = 0.15–0.54 m s^{-1}), while the cross-shelf component alternated sign (mean = 0.11 ± 0.07 m s^{-1}; range = −0.13 to 0.28 m s^{-1}) (Fig. 2g). The barotropic tidal model TPXO9 for the same period reproduced the phasing and modulation of these oscillations however amplitude was lower (±0.092/±0.05 m s^{-1} for CS-TIDE/AS-TIDE) than the observed during the experiment (Fig. 2h), indicating interaction with the subjacent flow.

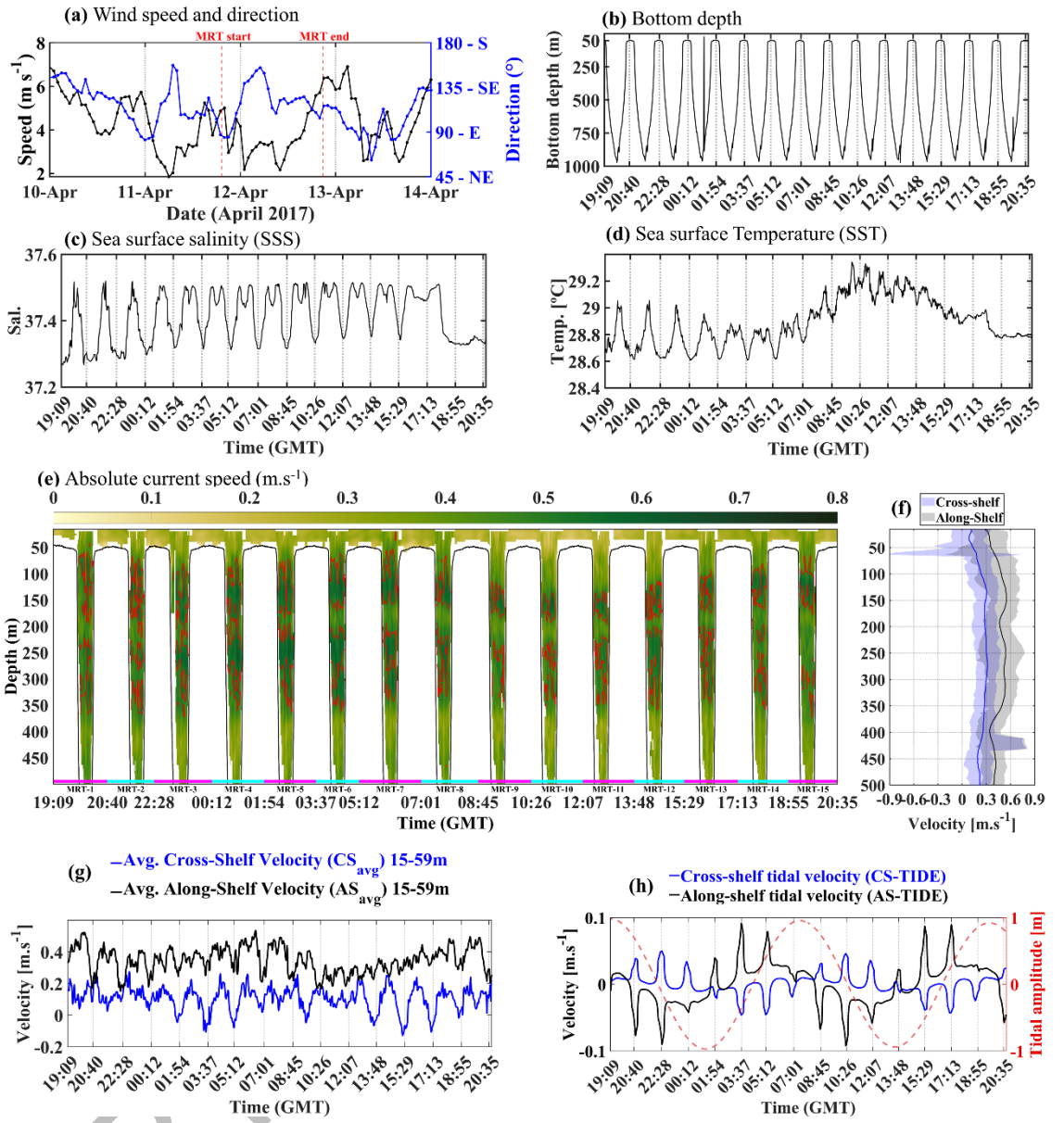

Figure 2. Synoptic forcing and currents during the MRT experiment (11–12 April; GMT). (a) Wind speed (black, m s^{-1}) and wind direction (blue, °; right axis). (b) Bottom depth (m) along the ship track. (c) Sea-surface salinity (psu).(d) Sea-surface temperature (°C). (e) Time–depth section (Hovmöller) of absolute current speed (m.s^{-1}) from shipboard ADCP; labels along the bottom mark the repetition of the transects MRT-1 to MRT15; the red line delineates the NBUC core, defined as speeds ≥ 70% of the maximum along-shelf flow. (f) Depth profiles of along-shelf (blue) and cross-shelf (black) velocities averaged over the experiment; shaded envelopes indicate variability (max./min.) across casts. (g) Layer-averaged velocities (15–59 m): along-shelf (black) and cross-shelf (blue). (h) Tidal currents from TPXO9: along-shelf (black) and cross-shelf (blue); red dashed curve (right axis) is tidal amplitude.

Tidal forcing dominated shallow current variability. EEMD revealed three main variability scales mostly related to tidal cycle: semidiurnal (C7/C8), shelf–ocean (C5), and shelf-break (C4) (Fig. 3a,b) with along-shelf energy peaking near high tide (Fig. 3c) and cross-shelf energy reducing when the along-shelf semidiurnal mode was weaker (Fig. 3d). Indeed, along-shelf velocity was dominated by the semi-diurnal

period (≈36.1% of variance), consistent with the orientation of local M2/S2 tidal ellipses and phase of tidal amplitude (Fig. 1c). Furthermore, C5 band structured spatial exchanges: along-shelf shear across the MRT intensified near high tide (high/low tide in Fig. 4a,b), while cross-shelf signals alternated between convergence at flood and divergence at ebb (flood/ebb in Fig. 4c,d). Along-shelf energy also increased exactly in the slope/shelf transition near high tide while tidal influence in this transition was weaker and sporadic for cross-shelf current (C4, Fig. 3a-b).

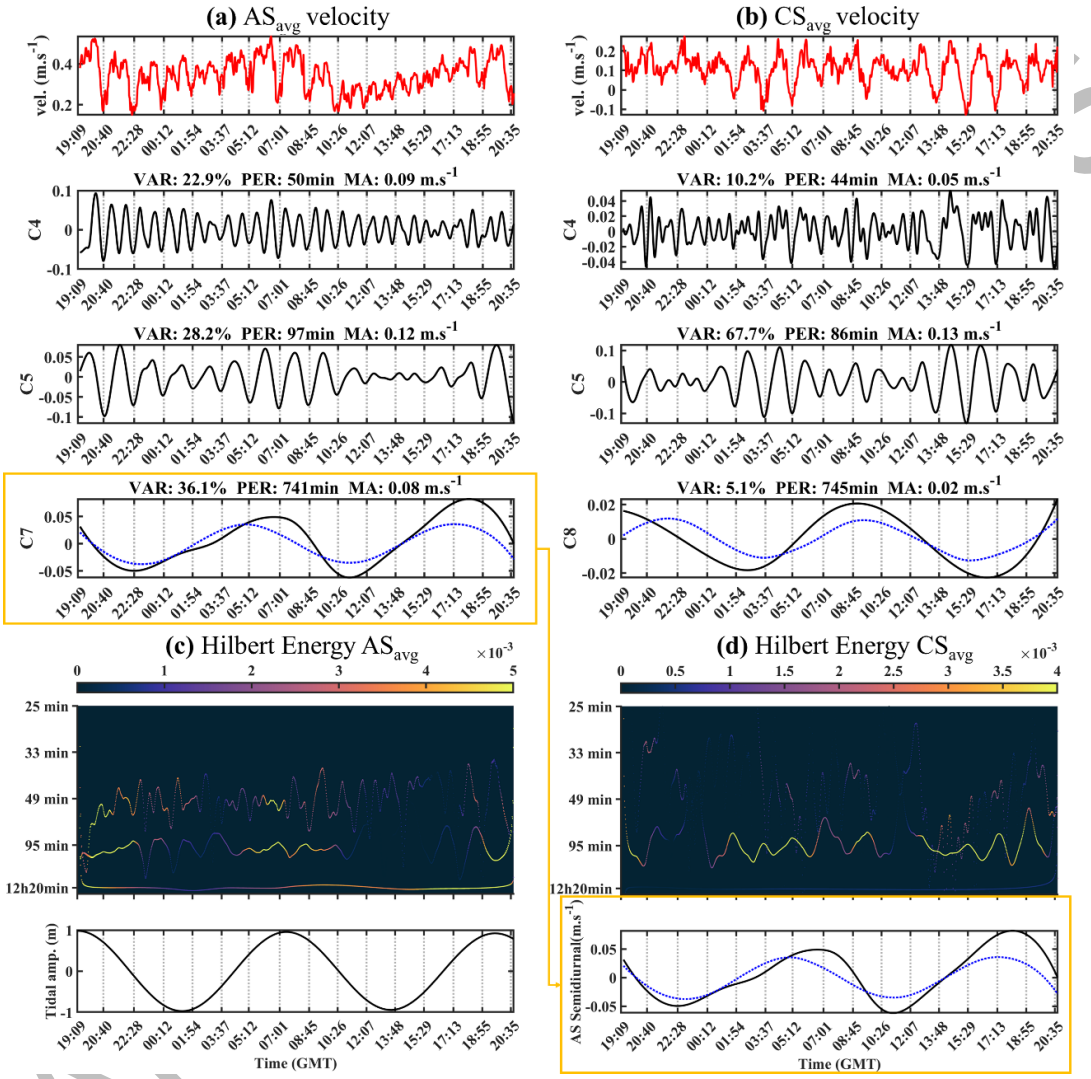

Figure 3. Decomposition of layer-averaged currents and time–frequency energy. (a) Along-shelf layer-averaged velocity (15–59 m; red) and its EEMD intrinsic mode functions (IMFs) highlighting three dominant bands: shelf-break scale (C4), shelf–ocean exchange scale (C5), and semidiurnal tide (C7). (b) Same as (a) for the cross-shelf component, with the semidiurnal tide captured by C8. For each IMF, VAR is the variance fraction, PER the characteristic period (min), and MA the mean amplitude (m s^{-1}). Blue dashed lines superimposed to semidiurnal modes are the along- and cross-shelf tidal currents from the TPXO9 tidal model, respectively in (a-b). (c–d) Hilbert energy spectra of the along-shelf (c) and cross-shelf (d) velocities showing time-evolving energy density across periods from ~25 min to ~12 h 20 min (warmer colors indicate higher energy). Lower insets show modeled tidal amplitude (c) and the extracted and modelled along-shelf semidiurnal mode (d) for reference. The panels together show semidiurnal dominance (≈36% of along-shelf variance), with along-shelf energy peaking near high tide and cross-shelf energy weakening when the along-shelf semidiurnal mode was weakest.

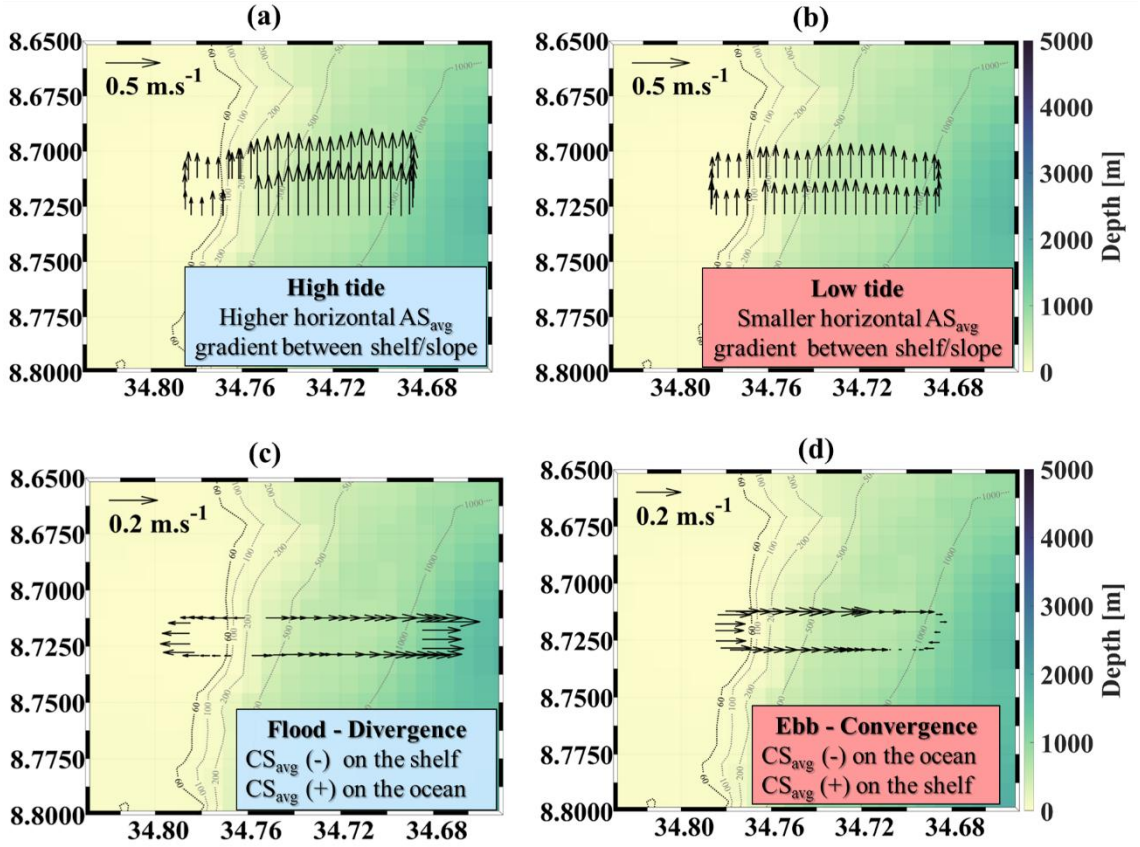

Figure 4. Snapshots of layer-averaged currents at key tidal stages. Maps show 15–59 m averaged velocity vectors plotted over bathymetry (color, m; gray isobaths). The arrow in the upper-left of each panel denotes the vector scale. (a) High tide: along-shelf flow exhibited a stronger horizontal gradient between shelf and slope. (b) Low tide: along-shelf gradient weakened across the shelf–slope transition. (c) Flood: cross-shelf pattern indicated divergence, with CS_{avg} negative (onshore-directed) on the shelf and positive (offshore-directed) offshore. (d) Ebb: cross-shelf pattern reversed to convergence, with CS_{avg} positive on the shelf and negative offshore.

THERMOHALINE STRUCTURE

The hydrographic casts documented a thermally stratified upper ocean overlying more homogeneous intermediate waters (Fig. 5). Near-surface salinity varied little among stations (generally ~37.1–37.3), so density structure largely mirrored temperature. A warm surface layer transitioned to a cooler thermocline whose depth and sharpness changed across the shelf–slope–ocean gradient. Over the shelf, the pattern ranged from a nearly homogeneous water column at ST1, with surface temperature ~28.7 °C, salinity ~37.3, density anomaly ~23.9 kg m^{-3}, weak stratification (N^2 mostly < 1 × 10^{-4} s^{-2}), and dissolved oxygen ~4.5–4.6 mL L^{-1}, to stations with a shallower and sharper pycnocline toward the bottom (ST8 and ST10). The latter were ~0.5–1.0 °C cooler than ST1 near the base of the profiles, consistent with intermittent intrusion of cooler subsurface waters. Off-shelf stations showed mixed-layer depths of ~40 m at ST2 and ~56 m at ST6, with N^2 maxima centered near 41 m and 66 m, respectively, reaching ~6.9–7.2 × 10^{-4} s^{-2}. Potential density increased from ~23.8–23.9 kg m^{-3} at the surface to ~25.6–26.5 kg m^{-3} by 100–160 m. Dissolved oxygen was ~4.5–4.6 mL L^{-1} in the surface layer, showed only modest vertical variation through the upper water column, and remained near ~4.5 mL L^{-1} at 200–300 m offshore. Fluorescence revealed a pronounced subsurface chlorophyll maximum within the upper thermocline, centered near ~94 m at ST2

and ~103 m at ST6, with peak values of ~0.94 and ~0.82 mg m^{-3}, respectively. In the shallowest and more weakly stratified profile (ST1), fluorescence remained low throughout the sampled water column (<0.16 mg m^{-3}), whereas stations showing cooler near-bottom signatures over the slope, such as ST8, also exhibited enhanced fluorescence in the upper pycnocline (~0.45 mg m^{-3}). The XBT profiles (rightmost column) reinforced these patterns across the shelf-break to oceanic transition. The profiles indicate a deeper thermocline offshore and comparatively shallower stratification near the shelf break, while also showing that the post-MRT high-tide cast (XBT5) was ~1–2 °C cooler at ~60 m than the nearby low-tide casts (XBT1 and XBT3) acquired less than 5 km away.

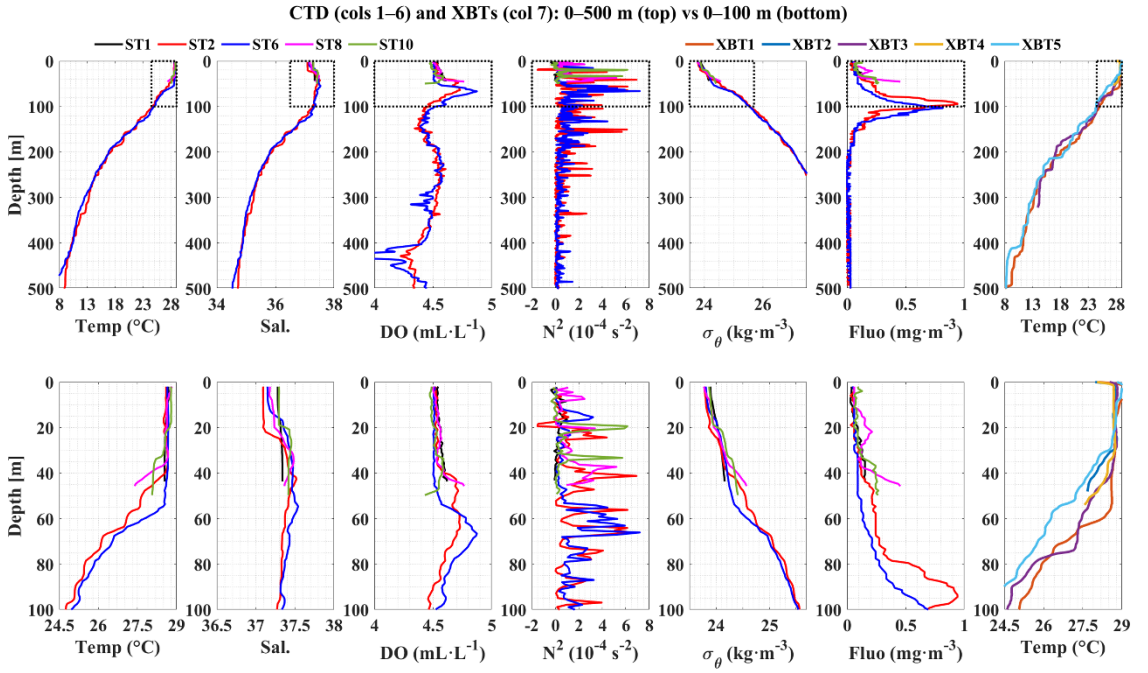

Figure 5. Hydrographic profiles from CTD stations and XBTs. Columns 1–6 show CTD profiles at shelf, shelf-break, and upper-slope stations (ST1, ST2, ST6, ST8, ST10; colors in legend). Column 7 shows XBT profiles (XBT1–XBT5). Variables from left to right are temperature, salinity, dissolved oxygen (DO), buoyancy frequency N^2, potential density σ_θ, and chlorophyll-a fluorescence. The top row displays the 0–500 m range; the bottom row zooms into the 0–100 m upper ocean (the dashed rectangles in the top row indicate the zoomed windows). Axes are consistent across columns to allow direct comparison among stations and instruments.

BIOLOGICAL SSLS

The acoustic data revealed the vertical distribution of acoustic groups (fish, fluid-like, and gelatinous), primarily dominated by the diel cycle. The sunset started at 19:00 (GMT) on April 11th and 12th until approximately 21:30, sunrise started at approximately 07:10 on April 12th and ended at 09:35m. The echograms for the MRT time series exhibit classic diel behavior, with higher acoustic biomass in the upper layers at night, mostly on the shelf and on the ocean down to ~200 m, than during the day (Fig. 6a).

At night, the current speed appeared to have no effect on the distribution of organisms in the water column (Fig. 6b), despite the current exceeding 0.6 $m.s^{-1}$ below 100 m. This vertical distribution in the upper 200 m likely results from prey availability and maximum chlorophyll-a concentrations. After dawn, a discernible migration cloud formed around 5:45 (Fig. 6a) until 8:45 when part of the organisms migrated to greater depths. A delayed migration cloud was also observed at the end of the sunrise (Fig. 6c)

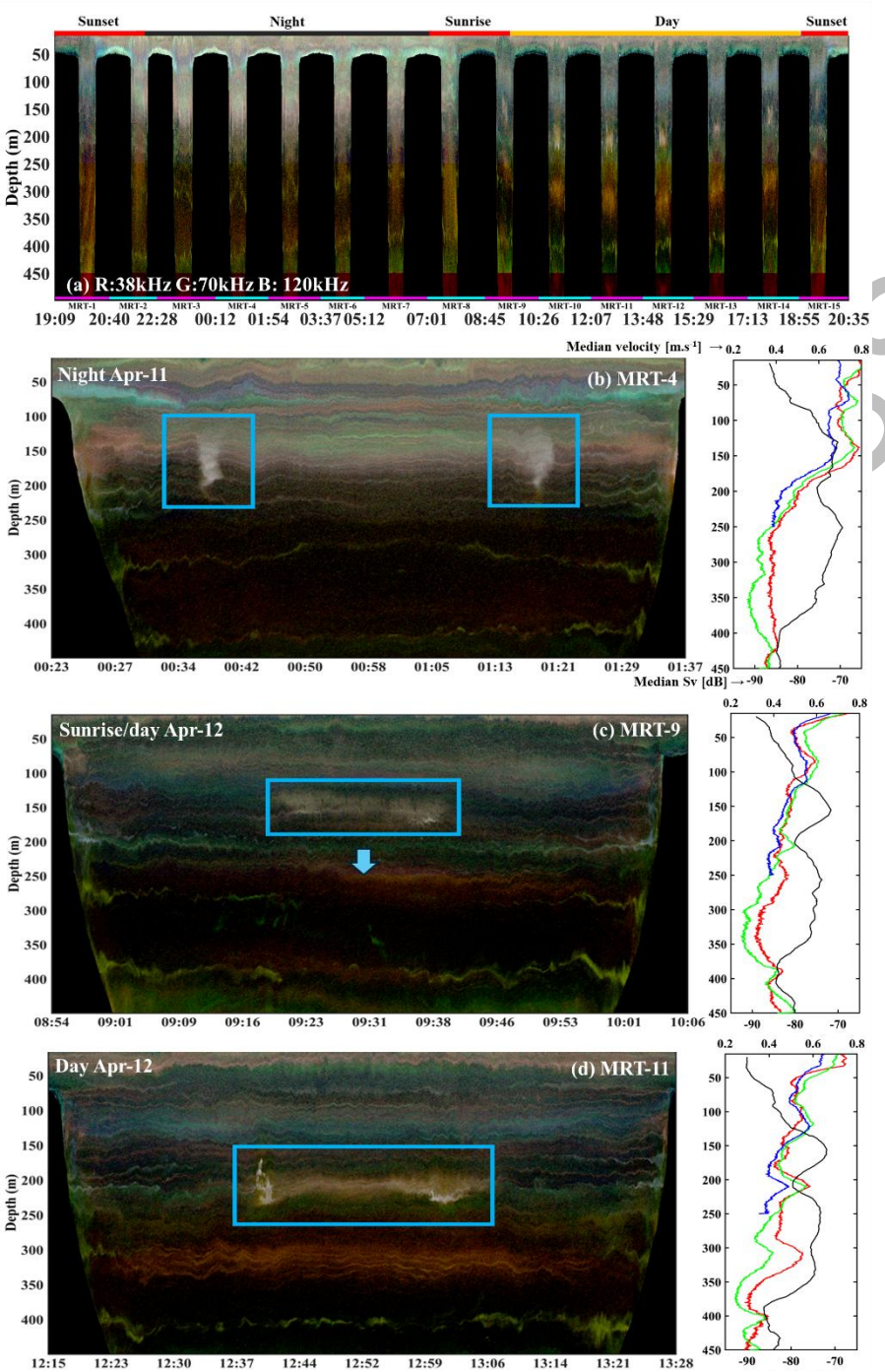

Figure 6. Multi-frequency RGB echograms and diel behavior of scatterers during the MRT sequence. (a) Composite RGB echogram of the entire record (0–500 m); colors map acoustic frequencies as R = 38 kHz, G = 70 kHz, B = 120 kHz. The alternating magenta/cyan ticks along the bottom mark successive casts MRT-1 through MRT-15 repetitions; the strip at the top indicates local light phases (sunset, night, sunrise, day, sunset). (b) MRT-4 (night, 11 Apr), (c) MRT-9 (sunrise/early day, 12 Apr), and (d) MRT-11 (day, 12 Apr) shown at higher resolution. Cyan boxes delineate discrete fish-like acoustic aggregations illustrating diel vertical migration. Here, 'fish-like' refers to targets with relatively homogeneous multifrequency responses and to acoustic patterns that are consistent with fish-dominated/gas-bearing aggregations, as further supported by the targeted trawls shown in Figs. 7 and 8, but not taxonomically validated on

a one-to-one basis. Right-hand panels display, for each cast, the median current speed (black curve, m s^{-1}; top axis) and the volume backscattering strength Sv profiles for each frequency (38 kHz = red; 70 kHz = green; 120 kHz = blue; bottom axis, dB).

During the day, off shelf organisms vertical distribution appeared to be influenced by currents, as evidenced by the separation of the SSLs in response to the current field (e.g., MRT-11 in Fig. 6d). The observed pattern below 100 m showed an increase in acoustic biomass as current velocity decreased. Specifically, one SSL around 100 m, remained above the current peak of 0.6 m.s^{-1} even when the current speed increased with high tide.

Another SSL, centered around 205m, appeared only during the daytime, corresponding to organisms that migrated downward later in the sunrise (Fig. 6c,d) and coinciding with the local decrease in current speed within the NBUC's core (Fig. 2e). The subset of the discrete grey-to-white backscatter displayed a relatively homogeneous response across 38, 70, and 120 kHz, consistent with fish-like or gas-bearing targets in the broad sense used in multifrequency acoustic studies (Benoit-Bird, 2001). Two similar fish-like/gas-bearing SSLs (Fig. 7) were sampled through targeted pelagic trawls collected during the same ABRAÇOS 2 survey. One trawl, conducted just after the MRT, targeted echoes between 85 and 135 m and caught mainly carangiform fishes (*Selar crumenophthalmus*, *Decapterus punctatus*, *Decapterus tabl*) and smaller myctophiform fishes (Diaphus, Lepidophanes, Benthosema). Another trawl, conducted before the MRT, targeted echoes around 240–260 m and caught mainly Lepidophanes, the mackerel-like fishes *Pseudoscopelus cordilluminatus* and *Taractichthys longipinnis*, and fish larvae.

The fish-like/gas-bearing echoes were observed during sunset on the shelf edge as individual targets that disappeared during the night and a large pelagic shoal (not shown). Later in the night (~2:00 GMT), this shoal began to disperse, with echoes appearing more diffuse on the echogram (Fig. 6b). During sunrise, it started to regroup, and the resulting aggregation migrated downward (MRT-9, Fig. 6c), completing the migration later than the main migration cloud. Additionally, the shoal did not migrate to deeper waters like most of the migrants, settling in the layer around 205 m (MRT-11, Fig. 6d) also began its upward migration early (not shown), almost 1 hour prior to the second day's sunset.

Lastly, two other stronger SSLs were observed below 300 m: The first one (~310 m) coincided with a small decrease in current speed and the second (~400 m) with a larger decrease due to its location below the NBUC's core (Fig. 6d). The layers also matched depth of the low oxygen zones at ST6 (Fig. 5).

DISCUSSION

During the MRT experiment we observed interesting features and patterns that need a closer look: (i) NBUC and biological association, (ii) tidal dominance over shallow cross- and along-shelf currents; (iii) uplift variability.

LOCALIZED WEAKENING OF THE NBUC CORE

The along-shelf current values, representative of the NBUC, were consistent with the seasonal characteristics reported in previous studies (Silva et al., 2009a,b; Veleda et al., 2011; Dossa et al., 2021a). However, the observations also revealed a locally weakened-current structure within the NBUC core that, to our knowledge, has not been previously described for this region, likely because of the finer observational and processing scales used here. This layer produced a marked shear band (not shown), similar to the features observed in another WBC system, the Kuroshio Current, where internal wave

propagation was suggested as a possible mechanism (Nagai et al., 2017). Although this comparison is useful, the present data do not allow us to determine whether internal wave propagation or another process is responsible for the structure observed here.

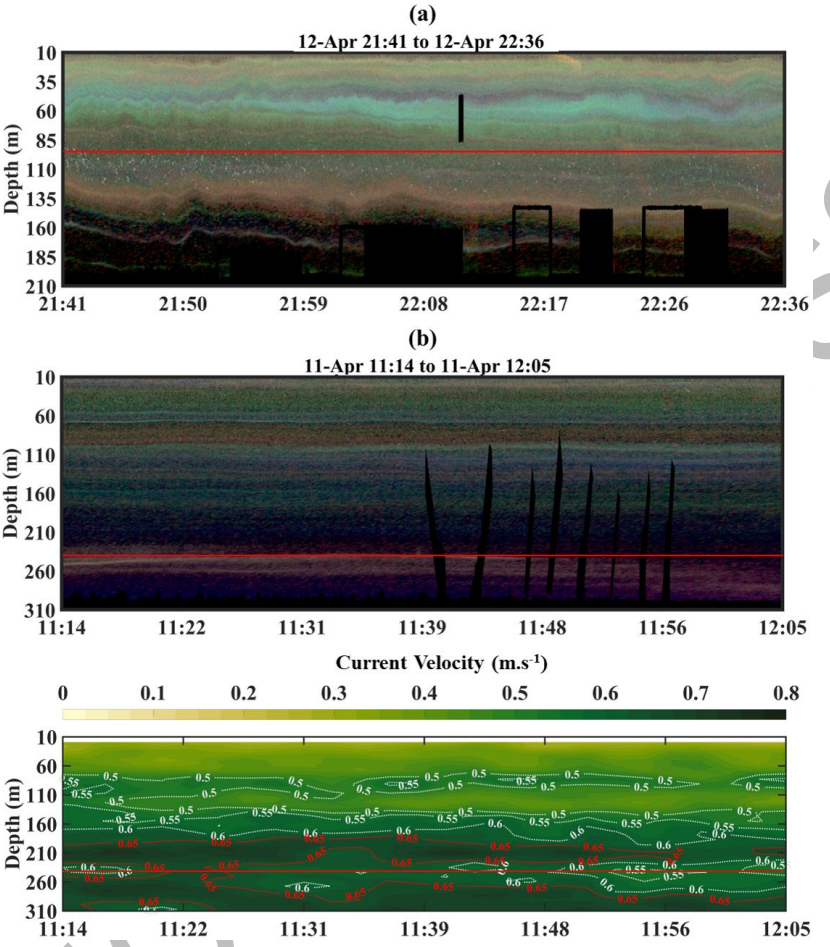

Figure 7. Targeted pelagic micronekton trawls on acoustically similar fish-like layers during the ABRAÇOS 2 survey. (a) RGB echogram acquired immediately after the Multiple Rectangles Transect experiment along transect A9–B9 (Fig. 1), from 12 April 2017, 21:41 to 22:36. The red line indicates the target depth of a pelagic micronekton trawl deployed at 21:51 to sample fish-like acoustic echoes between 85 and 135 m. The trawl had a 24 × 24 m mouth opening, 40 mm body mesh, and 10 mm cod-end mesh, and was towed for approximately 35 min. The catch was dominated by Carangiformes, including Selar crumenophthalmus, Decapterus punctatus, and Decapterus tabl, together with Myctophiformes of the genera Diaphus, Lepidophanes, and Benthosema. (b) RGB echogram and current velocity acquired before the MRT experiment along transect A6–B6 (Fig. 1), from 11 April 2017, 11:14 to 12:05. The red line indicates the target depth of a pelagic micronekton trawl deployed at 11:24 to sample acoustic echoes between 240 and 260 m. The same trawl configuration was used, with an approximate towing duration of 30 min. The catch was dominated by Myctophiformes (Lepidophanes), scombriform fishes including Pseudoscopelus cordilluminatus and Taractichthys longipinnis, and fish larvae. The figure provides biological support for the interpretation that acoustically similar layers in the region can be fish-dominated.

Because no previous high-resolution measurements were available for this region, we used ancillary reanalysis products to examine whether a comparable weakened-current structure could be inferred at broader scales near the MRT, along sections at 9.25°S, 8.75°S, and 8.25°S (Fig. 8a-c), with the 8.75°S section

located closest to the MRT.

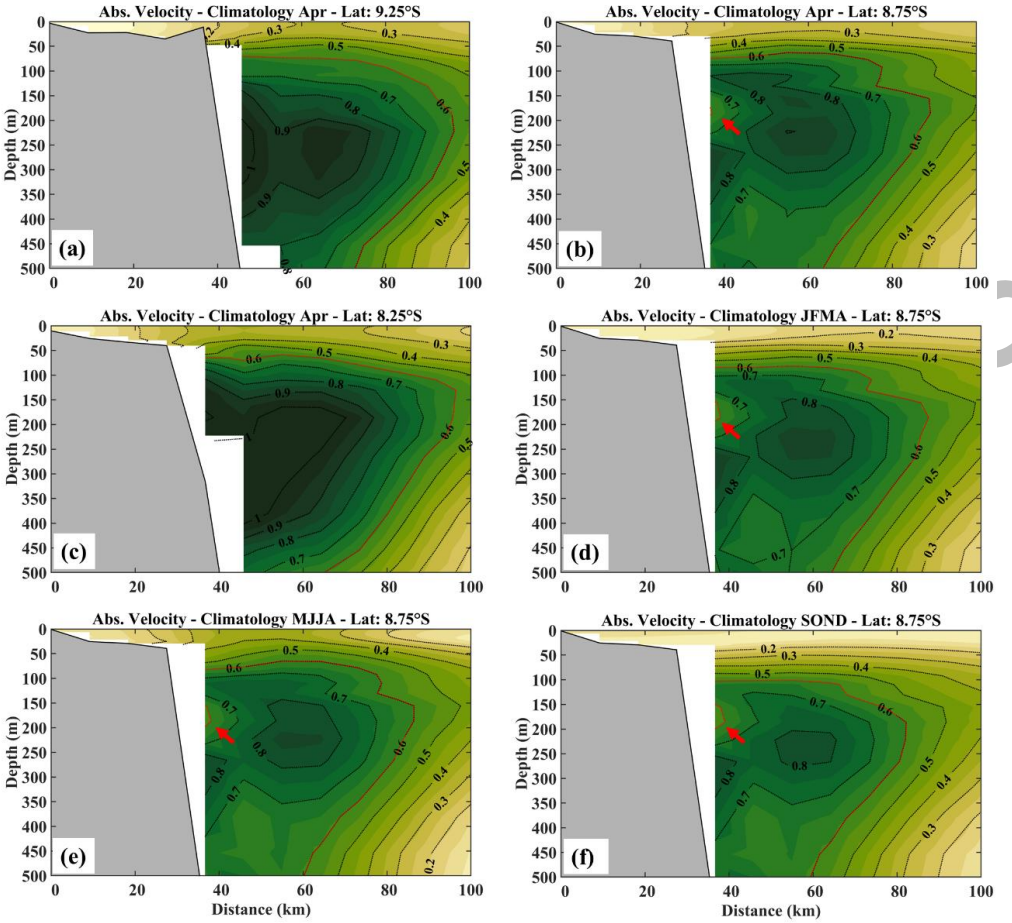

Figure 8. Zonal sections from the shore to 100 km offshore for current velocity climatology from Global Ocean Physics Reanalysis from 1993 to 2016 of the Copernicus Marine Service (https://doi.org/10.48670/moi-00021). April cross-sections for current velocity at (a) 9.25°S, (b) 8.75°S and (c) 8.25°S. 4-month averaged current velocity cross-section at 8.75°S from (d) January to April, (e) May to August and (f) September to December. The core location ~0.6 m.s^{-1} is indicated by the red isoline superimposed on the absolute velocity. The red arrow in the cross-sections around 8.75°S in (b) and (d,f) indicates the lower current zone within the NBUC's core close to the slope.

These climatological fields suggest that a weaker NBUC core may be a local feature, occurring only in the transect closest to the study area. The fact that a similar pattern appears throughout the year in the climatological fields (Fig. 8d–f) is consistent with, but does not demonstrate, a stationary mechanism, possibly related to flow–topography interactions. However, this inference must be treated cautiously, because the spatial resolution of the hydrodynamic reanalysis and the smoothed representation of bathymetry on the model grid are the main limitations of this dataset. Therefore, although topographic datasets such as ETOPO1 – used as a boundary condition for the GLORYS model –can depict regional bathymetric structures, small-scale bathymetric gradients and local flow–topography interactions may not be dynamically resolved by the reanalysis fields. Topographic structures represented at broader scales, such as deep channels and/or the Gaibu High (Fig. 1a), may contribute to the formation of this weakened-current zone. Another possibility is that slope irregularities modify the local isobath orientation and partially detach the current from the slope, creating a sheltered region of lower velocity. Since the scope

and resolution of the present study do not allow further determination of the responsible mechanism, we emphasize the need for future process-oriented experiments specifically designed to investigate flow–topography interactions in this region. Therefore, rather than interpreting this structure as a fully proven persistent anomaly, we consider it a locally observed feature whose broader temporal persistence is only suggested by the climatological setting. Any ecological implication, such as its possible role as a recurrent refuge for vertically migrating organisms, should be understood in this more cautious context.

NBUC WEAKENING AND BIOLOGICAL SSLS

As indicated by our MRT results, the nighttime distribution of the SSLs does not appear to be primarily controlled by currents. During the night, organisms occupied the upper part of the water column despite current speeds exceeding 0.6 m s^{-1} below 100 m, suggesting that other factors, such as prey availability and the deep chlorophyll maximum centered near 100 m, were more important in structuring their vertical distribution at that time. In contrast, during the day the vertical organization of the off-shelf scatterers became more clearly related to the current field. One SSL remained around ~100 m, above the current maximum, while another, centered near ~205 m, coincided with the weakened-current layer inside the NBUC core. In addition, from daytime to sunset, fish-like echoes were observed at the shelf edge as individual targets that disappeared during the night, consistent with diurnal demersal reef fishes (Eduardo et al., 2018; Salvetat et al., 2022).

Within the scope of the MRT, therefore, the clearest direct observation was the repeated daytime association between a fish-like acoustic aggregation and the weakened-current layer near ~205 m in the core of the NBUC. This pattern was observed continuously along the repeated transects, with the aggregation becoming organized during sunrise and remaining concentrated during the day in the lower-velocity portion of the undercurrent core. Two targeted pelagic micronekton trawls conducted during the same ABRAÇOS 2 survey on acoustically similar fish-like layers provide additional biological support for interpreting such echoes as fish-dominated, although they do not constitute one-to-one validation of the specific MRT aggregation because they were not taken on the exact shoal tracked during the MRT. For this reason, and because multifrequency acoustics alone do not uniquely resolve species composition in diverse mesopelagic systems, we refrain from assigning species identity to the MRT targets themselves. Instead, we interpret the ~205 m aggregation conservatively as a likely fish-dominated mixed assemblage rather than a taxonomically resolved school.

At the broader ABRAÇOS 2 survey scale, but outside the MRT itself, Assunção et al. (2023) analyzed multifrequency acoustics, hydrography, and SADCP-derived currents around CTD stations across the western boundary current system and the South Equatorial Current system and concluded that organisms tend to avoid strong current cores. That study, however, was based on station-centered analyses, with current profiles averaged over a radius around each CTD station, and therefore did not resolve the continuous spatial and temporal variability captured by the MRT at the shelf-break. Still, it provides important regional context for our observations. In particular, sampled layers between 200 and 300 m during the ABRAÇOS 2 surveys in the NBUC system revealed the presence of both invertebrates, including Ctenophora and Cnidaria, and fishes, including lanternfishes, hatchetfishes, and fish larvae (Assunção et al., 2023). This broader survey context is compatible with the interpretation that the ~205 m MRT layer may have contained a mixed assemblage rather than a single taxonomic group.

The biological interpretation can be further refined using the ABRAÇOS 2 taxonomic studies. Eduardo et al. (2021) showed that the ABRAÇOS 2 survey identified 33 Myctophidae species in the SWTA, of which 30 are likely to possess swim bladders, whereas Eduardo et al. (2020) showed that none of the identified

Sternoptychidae species have swim bladders. This distinction is relevant because the discrete grey-to-white echoes observed in the MRT RGB echograms are consistent with fish-like targets that may include gas-bearing fishes. Myctophidae are also known to migrate early (Catul et al., 2011), and Eduardo et al. (2021) attributed the vertical distribution of lanternfishes in the upper mesopelagic layer of the SWTA to their ability to actively select favorable vertical layers and environmental conditions. In this sense, the weakened-current layer observed within the NBUC core during the MRT may represent one such favorable layer. At the same time, this does not exclude a mixed composition, since other fish groups can generate similar fish-like backscatter.

Indeed, the MRT aggregation may also have included carangids. A pelagic trawl conducted on the night after the MRT at ~100 m depth, where similar echoes were detected, was dominated by the round scad *Decapterus punctatus* and the rough scad *Decapterus tabl* (Fig. 7a). Moreover, the gregarious behavior observed in the echograms resembles that described for the closely related jack mackerel *Trachurus murphyi* in the Peruvian eastern boundary system (Bertrand et al., 2006), although it was never observed in western boundary systems. Within the MRT itself, fish-like targets were more loosely distributed at night around ~150 m, coinciding with a SSL within the NBUC core. At sunrise they began regrouping and migrating downward, and during the day they concentrated in the reduced-velocity region where the dense ~205 m SSL was observed. A second trawl performed closer to the slope but farther from the MRT also intercepted a layer associated with decreased velocity within the NBUC core and was composed primarily of lanternfishes and mackerels (Fig. 7b), which further supports the hypothesis that acoustic similar layers in this sector can be composed of mixed fish assemblages.

From a physical perspective, the MRT observations are consistent with the idea that the shelf-break and slope form a favorable aggregation environment. Despite the strong along-shelf advection imposed by ocean currents (Brink, 2016), regions with high topographic gradients tend to aggregate zooplankton and fishes (Boehlert and Mundy, 1993; Genin, 2004). Such regions can disrupt geostrophic balance and induce upwelling, creating favorable conditions for primary productivity and prey availability (Pingree et al., 1981; Boehlert and Mundy, 1993; Genin et al., 2005). Here, upwelling refers to the upward displacement of colder subsurface waters up to the surface, whereas uplift refers to their shoaling toward shallower depths without reaching the surface (after Rochford, 1991). In the SWTA, uplift associated with the slope has already been described south of 10°S (Silva et al., 2022), indicating that the region sampled by the MRT is likely a favorable aggregation zone. Under these conditions, micronekton may benefit from remaining near the slope while using localized low-current regions to reduce advection.

The MRT results further suggest that reduced-current zones inside the NBUC can act as hydrodynamic refuges. The concentration of the ~205 m aggregation within the weakened-current layer is consistent with the idea that micronekton selectively occupies areas of reduced flow to lower energy expenditure while continuing their vertical migrations. This interpretation agrees with previous studies showing that aquatic organisms balance the trade-off between energy expenditure and resource acquisition by selecting hydrodynamically favorable habitats (e.g., Boehlert and Mundy, 1988; Bennett et al., 2002; O'dor et al., 2002; Kelly and Klimley, 2012). Although few studies have directly addressed the relationship between currents and fish behavior (e.g. O'dor et al., 2002; Assunção et al., 2023), the broader literature highlights the behavioral plasticity and environmental adaptations of deep-pelagic fishes (Gjøsaeter and Kawaguchi, 1980; Yancey et al., 1989; Neilson and Perry, 1990; Sutton and Hopkins, 1996; Langbehn et al., 2019; Romero-Romero et al., 2019; Aparecido et al., 2023; Eduardo et al., 2024). In this context, it seems reasonable that organisms associated with the NBUC may exploit current flaws to conserve energy while maintaining access to the productive and prey-rich environment of the slope vicinity. Likewise, the upper

daytime SSL around 100 m, which is consistent with fluid-like backscatter in the sense discussed by Assunção et al. (2023), also appeared to avoid the strongest currents, moving upward or downward as the current layer below strengthened or weakened with the tides.

For the deeper SSLs, however, the role of currents remains less clear. The third layer, between 300 and 400 m, was not sampled during ABRAÇOS 2, which makes its biological composition difficult to infer. In addition, the reduction in current speed at that depth was not as stable or as pronounced as the one observed near 205 m. The 400–500 m sampled layer, located below the NBUC and within the local oxygen minimum, contained invertebrates such as Cnidaria, Ctenophora, and Crustacea, gelatinous organisms such as Pyrosomidae, and deep fishes from the order Stomiiformes (Assunção et al., 2023). Since marine organisms often aggregate in cooler and lower-oxygen waters that may function as refuge or energy-saving habitats (Bertrand et al., 2006; Sutton, 2013), and because these layers can further depress oxygen through respiration (Bianchi et al., 2013), it is plausible that the deeper daytime SSLs were influenced more strongly by oxygen structure than by the current field. This is consistent with previous studies showing that deep SSLs frequently coincide with relatively hypoxic depths (e.g., Bianchi et al., 2013; Cade and Benoit-Bird, 2015; Klevjer et al., 2016; Assunção et al., 2023).

More broadly, ABRAÇOS was not the first project to investigate SSLs off northeastern Brazil. A previous acoustic survey conducted during May and June 2004 as part of the REVIZEE program (Weigert and Madureira, 2011) reported higher concentrations of organisms between the surface and ~200 m and again below 500 m, with relatively sparse occupancy between 200 and 500 m. In contrast, the MRT revealed substantial concentrations within this intermediate depth range. One possible explanation is that the earlier survey did not sample low-current zones associated with the NBUC; however, this remains uncertain because co-located current measurements were not presented together with the acoustic observations in that study.

Finally, our results raise the broader question of whether similar stable low-velocity zones occur within the core of other western boundary currents, and how marine organisms may exploit them in other regions. The climatological analyses suggest that the weakened NBUC core observed near the MRT may be a persistent local feature, likely linked to flow-topography interactions, and therefore may provide a recurrent refuge for vertically migrating organisms. Future work should therefore focus on regions with strong bathymetric variability, such as slope corrugations, canyons, plateaus, and submarine banks, where current–topography interactions may generate comparable low-current zones and influence biological distributions on fine scales.

TIDAL DOMINANCE OVER SHALLOW CROSS- AND ALONG-SHELF CURRENTS

As indicated by our results, during MRT experiment under weak-wind forcing (Fig. 2a), the upper-ocean variability was governed primarily by tidal forcing. As pointed out by Brink (2016), little is known about the general cross-shelf flow components and mechanisms in the SBSs due to their complexity and variability in time and space. During the MRT experiment we obtained time and space varying current data that revealed the alternation of the cross-shelf current between shelf-ward and ocean-ward, creating patterns of convergence and divergence (Fig. 4). In previous work by Domingues et al. (2017) a persistent cross-shelf flow towards the coast was previously reported at the region under the influence of the Pernambuco Plateau topography (Fig. 1b), but no mechanism was proposed for this flow until now.

Although wind is a known driver of shelf-break dynamics (Allen, 1980; Lentz, 2001; Lentz and Chapman, 2004), in cases where the wind is weak, as observed during the MRT experiment, other processes may be responsible for the cross-shelf patterns (Dever, 1997; Schaeffer et al., 2013; Brink, 2016). Baroclinic

instabilities can also create cross-shelf exchanges due to horizontal density gradient compensation in shelf-break frontal dynamics (Barth et al., 1998; Cottier et al., 2005). Nevertheless, although the surface cross-shelf velocity variability resembles a shelf-break front at times, the sea surface temperature and salinity gradients were too small (amplitude of 0.73°C for SST and 0.25 for SSS) to be considered as fronts. The same can be said about undersurface temperature and salinity from CTD and XBT that do not present horizontal gradients as marked as those expected in frontal systems (e.g., Yanagi, 1987; Barth et al., 1998; Acha et al., 2004). Cross-shelf transport can also be induced by internal wave propagation (Pineda, 1994; Cacchione, 2002; Lamb, 2013); however, our dataset does not allow us to confirm if internal waves dynamic was in play during the MRT experiment.

Instead, our results suggest that tidal forcing is likely the main driver of observed cross-shelf patterns, as the same patterns were observed from the cross-shelf velocity from the tidal model. In the model, cross-shore variability seems to arise from the phase difference between the slope and the shelf-break (see tidal ellipses in Fig. 1c). This phase difference is known to result from bottom friction over changing bathymetry (e.g., Huthnance, 1973; Stern and Shen, 1975; Loder, 1980; Loder and Wright 1985) or, in the absence of bottom friction, from nonlinear effects (Robinson, 1981). Although we are discussing only one mode of variability, this mode represents more than 67% of the total cross-shelf variability, which can have implications for the cross-shelf transport of sediments and nutrients within the tidal cycle.

We also showed that tides played a role in changing along-shelf dynamics (i.e., NBUC) across scales (Fig. 3). The general picture during the MRT experiment is that the tidal forcing increases the energy of the along-shelf current (Fig. 4). In turn, this energy is transferred from the along-shelf current to the cross-shelf component, increasing the gradients of the observed cross-shelf ebb/flood patterns (Fig. 4). Indeed, the tendency of stronger along-shelf velocity at the shelf-break transition than over the surrounding shelf and oceanic waters can create zonal compensating fluxes (i.e., divergence in the zonal direction) (Matano and Palma, 2008) and increased horizontal shear can lead to the generation of residual cross-shelf flow (Brink, 2016). We observed horizontal gradients (i.e., horizontal shear) created by the faster along-shelf current on the oceanic side of the MRT – with additional tidal contribution during the flood – and slower current at the adjacent shelf. This might explain why the cross-shelf current variability observed during the MRT experiment was an order of magnitude higher than the tidal model prediction, although we cannot disregard that it also could be a result of tidal model underestimation, since global barotropic tide models may smooth small-scale shelf and shelf-break variability and their performance can vary regionally in shallow waters depending on local bathymetry and unresolved coastal processes (Egbert and Erofeeva, 2002; Zaron and Elipot, 2021).

UPLIFT VARIABILITY

In Northeast Brazil, uplift/upwelling was previously observed in higher latitudes (~13°S) (Aguiar et al., 2014; 2018; Thévenin et al., 2019) mainly forced by winds and the eddies. However, the uplift north of 10°S was only reported recently by Silva et al. (2022), who noted that the NBUC was most likely the main driving force. NBUC is a well-defined cyclonic current and in this region the stratification is weak ($N^2 = O(10^{-4})$; here and in Assunção et al., 2020). During the fall of 2017, the context of our MRT experiment, the NBUC core was shallow (Dossa et al., 2021a), facilitating interactions with shelf dynamics. While the upwelling of cyclonic surface currents was reported before in western boundary systems (e.g. Matano and Palma, 2008), the NBUC is an undercurrent which should limit its influence on the subsurface waters. This could explain why we observe uplift in April and upwelling in the austral winter climatology when the upper limit of the current shallows (left vs. right panels in Fig. 9). In addition, as we have demonstrated, the tides significantly

influence the shallow NBUC's dynamics and cross-shelf currents; thus, we should anticipate implications for uplift variability within a tidal cycle.

Theoretically, the uplift should increase at high tide, led by the intensification of the along-shelf velocity and decrease during low tide with the reduction of the along-shelf velocity – as indicated by XBT5 profile launched post-MRT during high tide. This profile showed a reduction of 1°C to 2°C at 60m depth compared to the profiles acquired during low tide (XBT3 and XBT1, Fig. 5). However, isotherm configuration of this profile during high tide agrees with the climatological patterns (Fig. 9a), indicating that tidal forcing during high tide does not increase uplift beyond climatological norms, but rather, tidal forcing during low tide might decrease uplift. Nevertheless, without long-term measurements we cannot be sure if these observations are sustained outside the scope of the MRT experiment executed during the full moon spring tide.

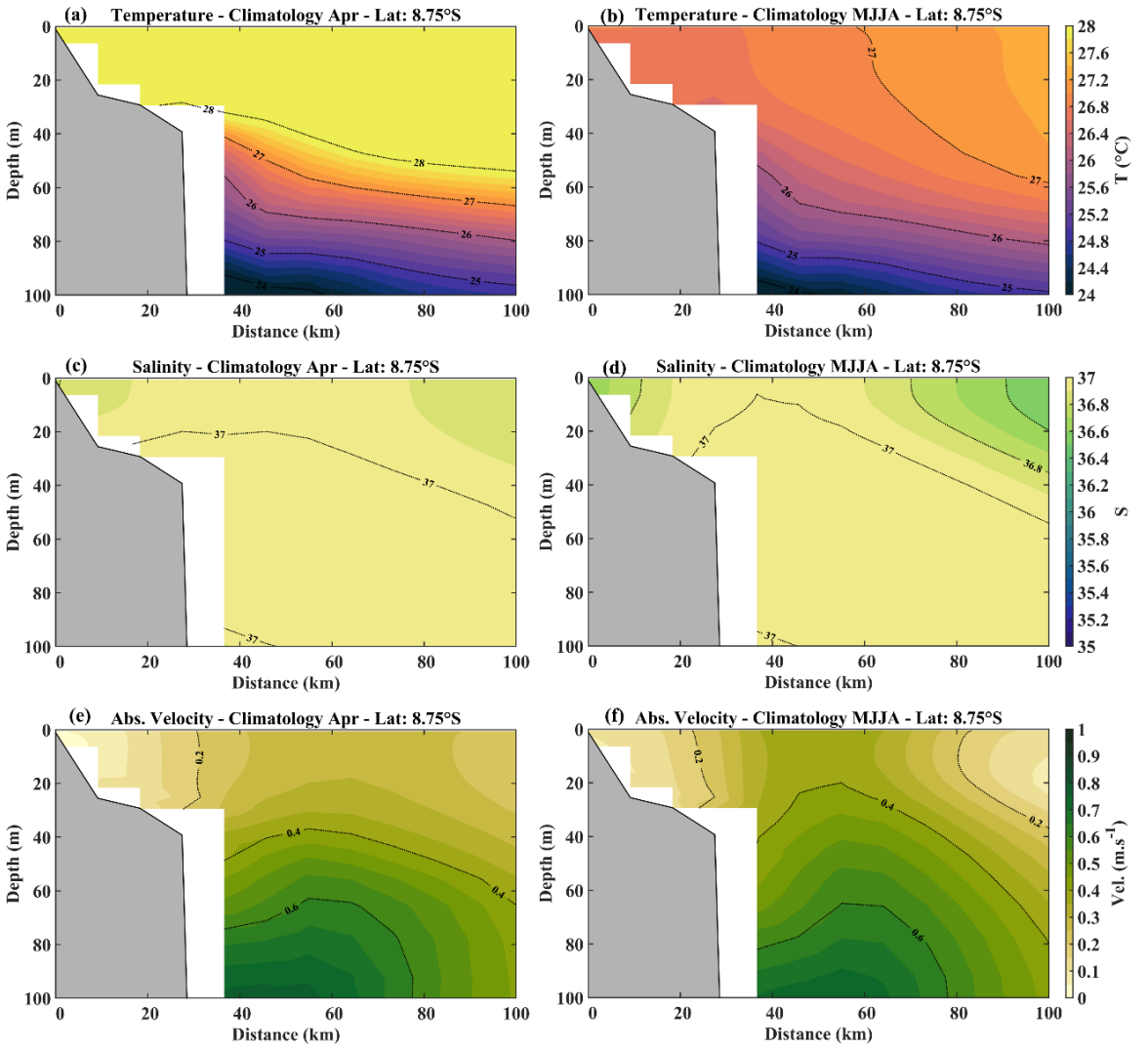

Figure 9. April (left panels) and May to August (MJJA, right panels) zonal sections from the shore to 100 km offshore and from 0-100 m for climatological (a,b) temperature, (c,d) salinity, and (e,f) absolute current velocity from Global Ocean Physics Reanalysis from 1993 to 2016 of the Copernicus Marine Service (https://doi.org/10.48670/moi-00021).

Despite that, the presence of colder water at the bottom layers of the shelf stations, coupled with

increased chlorophyll-a levels (Fig. 5), suggests that cross-shelf transport and variability play a significant role in enhancing primary productivity on the outer shelf. We should expect that during the flood, the shelf-ward transport of the uplifted is favored, as indicated by St. 8, conducted towards the end of an ebb period at high tide. With the euphotic layer down to 60-90 m depth (Macedo et al., 2009), uplift can enhance primary productivity, top predators and fisheries through bottom-up structuring (Bertrand, 2008b; 2014), enhancing the biological richness of the shelf-break/slope region. Indeed, despite historical classifications of these waters as oligotrophic (Ekau and Knoppers, 1999; Araujo et al., 2019), recent studies such as Eduardo et al. (2018) have documented higher-than-expected fish diversity and abundance near the shelf-break, specifically between depths of 30 and 60 m depth. The slope uplift along with the cross-shelf flow transporting enriched waters towards the shelf could elucidate why areas of high fish densities and diversity are located close to the shelf-break.

Lastly, we should also highlight that the comparison between the stations and selected profiles from the climatology showed that salinity from the CTD stations was higher than the climatology. A similar pattern was seen when comparing reanalysis products for April 11th with the CTD data (not shown). The same was observed from thermosalinograph salinity data when compared with SSS from the reanalysis. Quality information document for the GLORYS reanalysis product (Drévillon et al., 2023) report large fresh anomalies in tropical areas such as the western Atlantic and Pacific oceans. Silva et al. (2019b) also observed fresh anomalies in their simulation using ROMS and pointed out that the discrepancies are probably related to the model difficulty in reproducing the ventilation of subducted lower-thermocline waters coming from the subtropical South Atlantic Ocean. However, Dossa et al. (2021b) compared salinity from thermosalinograph data from ABRAÇOS 2 (without the MRT observations) with the same reanalysis product and concluded that the latter reproduces well the sea surface salinity cross-shore gradients. This indicates that the model's resolution might fail to capture local processes close to the shelf-break that are influencing salinity levels. Moreover, we cannot rule out the possibility that interannual variability or climatic changes may also be contributing to this difference.

CONCLUSION

This study leveraged high-resolution spatial and temporal data obtained from a process-oriented in situ observation experiment to explore hydrodynamic variability and current's physical structuring of marine organisms vertical distribution at the shelf-break and slope. A key strength of this study is the simultaneous use of acoustic and current data, allowing us to observe how marine organisms interact with oceanic physical structures. Additionally, advanced analytical techniques such as Ensemble Empirical Mode Decomposition and the Hilbert spectrum significantly strengthened the study by allowing for precise isolation and analysis of critical modes of variability. EEMD excels in analyzing signals where the frequency and amplitude may vary over time, which is characteristic of the tidal processes and other hydrodynamic phenomena observed in our study. This method adapts to the data's intrinsic characteristics without the need for predefined basis functions, allowing for a more faithful decomposition into intrinsic mode functions (IMFs). These IMFs reflect the true dynamic nature of the observed signals and provide a nuanced understanding of the contributions to shelf-break dynamics. Furthermore, EEMD's ability to isolate frequency components dynamically makes it particularly effective for the MRT dataset, which includes both temporal and spatial variation. The potential of the EEMD to capture both temporal and spatial variability of the MRT measurements is demonstrated by the C4 and C5 modes. Indeed, C4 and C5 modes could be confused with artifacts due to the MRT repetitions but rather reflect real spatial patterns

associated with the topographic features traversed during the experiment as confirmed by the tidal model results. These patterns appeared because of the interaction between the western boundary current NBUC and the tides, evidenced by increased energy in all three main modes of the along-shelf current during high tide and the resultant cross-shelf velocity. However, future MRT experiments should be regarded carefully since they can capture non-synoptic features due to the non-stationary nature of the sampling design.

The use of ship-mounted SADCP and thermosalinograph alongside a rosette-mounted CTD ensured the accurate capture of surface and depth-specific measurements. This methodological setup proved particularly effective in documenting transient phenomena and was bolstered by strategic coverage of key hydrodynamic features at the shelf-break. However, despite its effectiveness, the MRT experiment's brief duration and the requirement for co-located water column structure measurements pose limitations, potentially restricting the scope of inferences that can be drawn about uplift variability. We addressed this issue by integrating data from the TPXO9 tidal model and reanalysis data, enhancing the contextual understanding of tidal influences, enabling a broader interpretation of local observations. In future work, to address the limitations inherent to the MRT methodology, we recommend the adoption of an underway CTD equipped with a fluorescence sensor system. Unlike discrete sampling with a rosette-mounted CTD, an underway CTD facilitates continuous, high-resolution sampling of the water column as the vessel moves. This approach would provide a more comprehensive and continuous depiction of the thermohaline structure, essential for fully capturing the dynamic nature of hydrodynamic processes during brief experimental setups like the MRT. Extending the duration of the MRT experiment to at least 48 hours could also considerably enhance the dataset, enable more thorough analyses of diurnal cycles and capture additional tidal phases. Such an extension would allow for a more detailed investigation of the interactions between tidal currents and shelf-break dynamics across multiple tidal cycles, fostering a deeper understanding of these intricate systems. Still, in an ideal scenario, deploying a moored array across the shelf break and slope equipped with multiple instruments at various depths would offer the most complete understanding of these dynamic regions.

Finaly, while this study has significantly advanced our understanding of shelf-break slope dynamics and the interaction with marine organisms in short term, it also underscores the need for further research with extended observational periods and process-oriented surveys. Given the NBUC's role in the upper AMOC, cross-shelf exchanges are critically important for global fluxes, budgets, and their responses to climate change and human activities (Huthnance, 1995). Additionally, anomalous variability in cross-shelf exchanges may signal changes in the dynamics of adjacent Western Boundary Currents (Wu et al., 2012; Gawarkiewicz et al., 2018; Todd et al., 2019), reinforcing the need for high-resolution, long-term observations in the SWTA and in other WBC systems.

AI USE DISCLOSURE

Artificial intelligence tool (ChatGPT) was used exclusively to refine the English language. The content was carefully reviewed by the authors, who are fully responsible for the final version of the manuscript.

DATA AVAILABILITY STATEMENT

The quality controlled CTD datasets are freely available at SEANOE repository (https://doi.org/10.17882/76352). The quality-controlled sea surface temperature and salinity, XBT, current

profiles and bathymetric data obtained during the MRT experiment are available through request to the LMI-TAPIOCA/IRD principal investigator (arnaud.bertrand@ird.fr). Monthly oceanic fields of the Global Ocean Physics Reanalysis product (https://doi.org/10.48670/moi-00021), and hourly wind reanalysis product (https://doi.org/10.48670/moi-00185) are freely available at the Copernicus Marine Environment Monitoring Service.

ACKNOWLEDGMENTS

We acknowledge the French oceanographic fleet for funding the at-sea survey and the officers and crew of the R/V Antea for their contribution to the success of the operations during the ABRAÇOS cruises. We thank the Laboratory for Studies of Anthropogenic Impacts on Marine and Estuarine Biodiversity (BIOIMPACT/UFRPE) students and researchers for their support. We also thank the reviewers and the Editor-in-Chief for their constructive comments and recommendations, which helped improve the clarity and quality of this manuscript. This work is a contribution to the International Joint Laboratory TAPIOCA (www.tapioca.ird.fr).

FUNDING

S.Q. thanks the support of the National Council for Scientific and Technological Development (CNPq) through a PhD scholarship grant (140629/2020-3). M.A. thanks the Brazilian Research Network on Global Climate Change - Rede CLIMA (FINEP-CNPq 437167/2016-0) and the Brazilian National Institute of Science and Technology for Tropical Marine Environments - INCT AmbTropic (CNPq/FAPESB 565054/2010-4 and 8936/2011) for their support.

AUTHOR CONTRIBUTION

S.Q: Conceptualization; Investigation; Methodology; Software; Formal Analysis; Writing – original draft; Writing – review and editing.

R.V.A.: Investigation; Writing – original draft; Writing – review and editing

L.N.E.: Investigation; Writing – original draft; Writing – review and editing

A.C.S.: Resources; Project Administration; Writing – review and editing.

M.A.: Supervision; Resources; Project Administration; Writing – review and editing.

A.B.: Conceptualization; Methodology; Resources; Project Administration; Funding Acquisition; Writing – review and editing.

CONFLICTS OF INTEREST

The authors declare no conflicts of interest.

REFERENCES

Acha, E. M., Mianzan, H. W., Guerrero, R. A., Favero, M. and Bava, J. 2004. Marine fronts at the continental shelves of austral South America. *Journal of Marine Systems*, *44*(1–2), 83–105. DOI: https://doi.org/10.1016/j.jmarsys.2003.09.005

Aguiar, A. L., Cirano, M., Marta-Almeida, M., Lessa, G. C. and Valle-Levinson, A. 2018. Upwelling processes along the South Equatorial Current bifurcation region and the Salvador Canyon (13°S), Brazil. *Continental Shelf Research*, *171*, 77–96. DOI: https://doi.org/10.1016/j.csr.2018.10.001

Aguiar, A. L., Cirano, M., Pereira, J. and Marta-Almeida, M. 2014. Upwelling processes along a western boundary current in the Abrolhos–Campos region of Brazil. *Continental Shelf Research*, *85*, 42–59. DOI: https://doi.org/10.1016/j.csr.2014.04.013

Allen, J. S. 1980. Models of Wind-Driven Currents on the Continental Shelf. *Annual Review of Fluid Mechanics*, *12*(1), 389–433. DOI: https://doi.org/10.1146/annurev.fl.12.010180.002133

Aparecido, K. C., Frédou, T., Eduardo, L. N., Mincarone, M. M., Lima, R. S., Morais, M. F. da S. and Mérigot, B. 2023. Living in darkness: functional diversity of mesopelagic fishes in the western tropical Atlantic. *Frontiers in Marine Science*, *10*(September), 1–17. DOI: https://doi.org/10.3389/fmars.2023.1117806

Araujo, M., Noriega, C., Medeiros, C., Lefèvre, N., Ibánhez, J. S. P., Flores Montes, M., Silva, A. C. da and Santos, M. de L. 2019. On the variability in the CO2 system and water productivity in the western tropical Atlantic off North and Northeast Brazil. *Journal of Marine Systems*, *189*, 62–77. DOI: https://doi.org/10.1016/j.jmarsys.2018.09.008

Ariza, A., Lebourges-Dhaussy, A., Nerini, D., Pauthenet, E., Roudaut, G., Assunção, R., Tosetto, E. and Bertrand, A. 2023. Acoustic seascape partitioning through functional data analysis. *Journal of Biogeography*, *50*(9), 1546–1560. DOI: https://doi.org/10.1111/jbi.14534

Assunção, R. V., Silva, A. C., Roy, A., Bourlès, B., Silva, C. H. S., Ternon, J.-F., Araujo, M. and Bertrand, A. 2020. 3D characterisation of the thermohaline structure in the southwestern tropical Atlantic derived from functional data analysis of in situ profiles. *Progress in Oceanography*, *187*, 102399. DOI: https://doi.org/10.1016/j.pocean.2020.102399

Assunção, R., Lebourges-Dhaussy, A., da Silva, A. C., Roudaut, G., Ariza, A., Eduardo, L. N., Queiroz, S. and Bertrand, A. 2023. Fine-scale vertical relationships between environmental conditions and sound scattering layers in the Southwestern Tropical Atlantic. *PLOS ONE*, *18*(8), e0284953. DOI: https://doi.org/10.1371/journal.pone.0284953

Barth, J. A., Bogucki, D., Pierce, S. D. and Kosro, P. M. 1998. Secondary circulation associated with a shelfbreak front. *Geophysical Research Letters*, *25*(15), 2761–2764. DOI: https://doi.org/10.1029/98GL02104

Bennett, W. A., Kimmerer, W. J. and Burau, J. R. 2002. Plasticity in vertical migration by native and exotic estuarine fishes in a dynamic low-salinity zone. *Limnology and Oceanography*, *47*(5), 1496–1507. DOI: https://doi.org/10.4319/lo.2002.47.5.1496

Benoit-Bird, K. J. and Au, W. W. L. 2001. Target strength measurements of Hawaiian mesopelagic boundary community animals. *The Journal of the Acoustical Society of America*, *110*(2), 812–819. DOI: https://doi.org/10.1121/1.1382620

Bertrand, A., Barbieri, M., Gerlotto, F., Leiva, F. and Córdova, J. 2006. Determinism and plasticity of fish schooling behaviour as exemplified by the South Pacific jack mackerel Trachurus murphyi. *Marine Ecology Progress Series*, *311*(April), 145–156. DOI: https://doi.org/10.3354/meps311145

Bertrand, A., Gerlotto, F., Bertrand, S., Gutiérrez, M., Alza, L., Chipollini, A., Díaz, E., Espinoza, P., Ledesma, J., Quesquén, R., Peraltilla, S. and Chavez, F. 2008a. Schooling behaviour and environmental forcing in relation to anchoveta distribution: An analysis across multiple spatial scales. *Progress in Oceanography*, *79*(2–4), 264–277. DOI: https://doi.org/10.1016/j.pocean.2008.10.018

Bertrand, S., Dewitte, B., Tam, J., Díaz, E. and Bertrand, A. 2008. Impacts of Kelvin wave forcing in the Peru

Humboldt Current system: Scenarios of spatial reorganizations from physics to fishers. *Progress in Oceanography*, *79*(2–4), 278–289. DOI: https://doi.org/10.1016/j.pocean.2008.10.017

Bertrand, A., Grados, D., Colas, F., Bertrand, S., Capet, X., Chaigneau, A., Vargas, G., Mousseigne, A. and Fablet, R. 2014. Broad impacts of fine-scale dynamics on seascape structure from zooplankton to seabirds. Nature Communications, 5(1), 5239. DOI: https://doi.org/10.1038/ncomms6239

Bertrand, A. 2015. *ABRACOS cruise, RV Antea*. DOI: https://doi.org/10.17600/15005600

Bertrand, A. 2017. *ABRACOS 2 cruise, Antea R/V*. DOI: https://doi.org/10.17600/17004100

Bianchi, D., Galbraith, E. D., Carozza, D. A., Mislan, K. A. S. and Stock, C. A. 2013. Intensification of open-ocean oxygen depletion by vertically migrating animals. *Nature Geoscience*, *6*(7), 545–548. DOI: https://doi.org/10.1038/ngeo1837

Boehlert, G. W. and Mundy, B. C. 1988. Roles of Behavioral and Physical Factors in Larval and Juvenile Fish Recruitment to estuarine nursery areas. *American Fisheries Society Symposium* (pp. 1–67).

Boehlert, G. W. and Mundy, B. C. 1993. Ichthyoplankton assemblages at seamounts and oceanic islands. *Bulletin of Marine Science*, *53*(2), 336–361. Accessed: https://www.ingentaconnect.com/content/umrsmas/bullmar/1993/00000053/00000002/art00003#

Brink, K. H. 2016. Cross-Shelf Exchange. *Annual Review of Marine Science*, *8*(1), 59–78. DOI: https://doi.org/10.1146/annurev-marine-010814-015717

Cacchione, D. A., Pratson, L. F. and Ogston, A. S. 2002. The Shaping of Continental Slopes by Internal Tides. *Science*, *296*(5568), 724–727. DOI: https://doi.org/10.1126/science.1069803

Cade, D. E. and Benoit-Bird, K. J. 2015. Depths, migration rates and environmental associations of acoustic scattering layers in the Gulf of California. *Deep Sea Research Part I: Oceanographic Research Papers*, *102*, 78–89. DOI: https://doi.org/10.1016/j.dsr.2015.05.001

Camargo, J. M. R. de, Araújo, T. C. M. de, Maida, M. and Ushizima, T. M. 2007. Morfologia da plataforma continental interna adjacente ao município de Tamandaré, sul de Pernambuco - Brasil. *Revista Brasileira de Geofísica*, *25*(11), 79–89. DOI: https://doi.org/10.1590/S0102-261X2007000500008

Castelao, R. 2011. Intrusions of Gulf Stream waters onto the South Atlantic Bight shelf. *Journal of Geophysical Research*, *116*(C10), C10011. DOI: https://doi.org/10.1029/2011JC007178

Catul, V., Gauns, M. and Karuppasamy, P. K. 2011. A review on mesopelagic fishes belonging to family Myctophidae. *Reviews in Fish Biology and Fisheries*, *21*(3), 339–354. DOI: https://doi.org/10.1007/s11160-010-9176-4

Chiao, L.-Y. & Wang, Y.-H. 2004. Multiresolution Interpolation and Detiding of the ADCP Data. *Journal of Atmospheric and Oceanic Technology*, *21*(1), 122–134. DOI: https://doi.org/10.1175/1520-0426(2004)021<0122:MIADOT>2.0.CO;2

Cottier, F., Tverberg, V., Inall, M., Svendsen, H., Nilsen, F. and Griffiths, C. 2005. Water mass modification in an Arctic fjord through cross-shelf exchange: The seasonal hydrography of Kongsfjorden, Svalbard. *Journal of Geophysical Research: Oceans*, *110*(12), 1–18. DOI: https://doi.org/10.1029/2004JC002757

Coutinho, P. N. 1996. Levantamento do estado da arte da pesquisa dos recursos vivos marinhos do Brasil-Oceanografia Geológica. *Região Nordeste. Programa REVIZEE. Ministério Do Meio Ambiente, Dos Recursos Hídricos e Da Amazônia Legal (MMA). Brasília, 97pp*.

Dever, E. P. 1997. Wind-forced cross-shelf circulation on the Northern California shelf. *Journal of Physical Oceanography*, *27*(8), 1566–1580. DOI: https://doi.org/10.1175/1520-0485(1997)027<1566:WFCSCO>2.0.CO;2

Domingues, E. C., Schettini, C. A. F., Truccolo, E. C. and Oliveira Filho, J. C. 2017. Hydrography and currents on the Pernambuco Continental Shelf. *Revista Brasileira de Recursos Hidricos*, *22*(0). DOI: https://doi.org/10.1590/2318-0331.0217170027

Dong, C., Xu, G., Han, G., Chen, N., He, Y. & Chen, D. 2018. Identification of tidal mixing fronts from high-resolution along-track altimetry data. *Remote Sensing of Environment*, *209*(January), 489–496. DOI: https://doi.org/10.1016/j.rse.2018.02.047

Dossa, A. N., Silva, A. C., Chaigneau, A., Eldin, G., Araujo, M. and Bertrand, A. 2021a. Near-surface western boundary circulation off Northeast Brazil. *Progress in Oceanography*, *190*, 102475. DOI: https://doi.org/10.1016/j.pocean.2020.102475

Dossa, A. N., Alory, G., da Silva, A. C., Dahunsi, A. M. and Bertrand, A. 2021b. Global analysis of coastal gradients of sea surface salinity. *Remote Sensing*, *13*(13). DOI: https://doi.org/10.3390/rs13132507

Drévillon, M., Regnier, C., Lellouche, J. M., Garric, G., Bricaud, C. & Hernandez, O. 2023. CMEMS-GLO-QUID-001-030. Quality Information Document For Global Ocean Reanalysis Products GLOBAL-REANALYSIS-PHY-001-030. *Copernicus, Marine Environment Monitoring Service*, *November 2*(1.6). Accessed: https://documentation.marine.copernicus.eu/QUID/CMEMS-GLO-QUID-001-030.pdf

Eduardo, L. N., Frédou, T., Lira, A. S., Ferreira, B. P., Bertrand, A., Ménard, F. and Frédou, F. L. 2018. Identifying key habitat and spatial patterns of fish biodiversity in the tropical Brazilian continental shelf. *Continental Shelf Research*, *166*, 108–118. DOI: https://doi.org/10.1016/j.csr.2018.07.002

Eduardo, L. N., Bertrand, A., Mincarone, M. M., Santos, L. V., Frédou, T., Assunção, R. V., Silva, A., Ménard, F., Schwamborn, R., Le Loc'h, F. and Lucena-Frédou, F. 2020. Hatchetfishes (Stomiiformes: Sternoptychidae) biodiversity, trophic ecology, vertical niche partitioning and functional roles in the western Tropical Atlantic. *Progress in Oceanography*, *187*, 102389. DOI: https://doi.org/10.1016/j.pocean.2020.102389

Eduardo, L. N., Bertrand, A., Mincarone, M. M., Martins, J. R., Frédou, T., Assunção, R. V., Lima, R. S., Ménard, F., Le Loc'h, F. and Lucena-Frédou, F. 2021. Distribution, vertical migration, and trophic ecology of lanternfishes (Myctophidae) in the Southwestern Tropical Atlantic. *Progress in Oceanography*, *199*(February), 102695. DOI: https://doi.org/10.1016/j.pocean.2021.102695

Eduardo, L. N., Mincarone, M. M., Sutton, T. and Bertrand, A. 2024. Deep-Pelagic Fishes Are Anything But Similar: A Global Synthesis. *Ecology Letters*, *27*(9). DOI: https://doi.org/10.1111/ele.14510

Egbert, G. D. and Erofeeva, S. Y. 2002. Efficient Inverse Modeling of Barotropic Ocean Tides. *Journal of Atmospheric and Oceanic Technology*, *19*(2), 183–204. DOI: https://doi.org/10.1175/1520-0426(2002)019<0183:EIMOBO>2.0.CO;2

Ekau, W. and Knoppers, B. 1999. An introduction to the pelagic system of the North-East and East Brazilian shelf. *Archive of Fishery and Marine Research*, *47*(2/3), 113–132.

Erofeeva, S. 2022. TPXO9v2 and TPXO9-atlas-v5: two new global barotropic tide models. *2022 Ocean Surface Topography Science Team Meeting* (p. 178).

Gawarkiewicz, G., Todd, R., Zhang, W., Partida, J., Gangopadhyay, A., Monim, M.-U.-H., Fratantoni, P., Malek Mercer, A. and Dent, M. 2018. The Changing Nature of Shelf-Break Exchange Revealed by the OOI Pioneer Array. *Oceanography*, *31*(1), 60–70. DOI: https://doi.org/10.5670/oceanog.2018.110

Genin, A. 2004. Bio-physical coupling in the formation of zooplankton and fish aggregations over abrupt topographies. *Journal of Marine Systems*, *50*(1), 3–20. DOI: https://doi.org/https://doi.org/10.1016/j.jmarsys.2003.10.008

Genin, A., Jaffe, J. S., Reef, R., Richter, C. and Franks, P. J. S. 2005. Swimming Against the Flow: A Mechanism of Zooplankton Aggregation. *Science*, *308*(5723), 860–862. DOI: https://doi.org/10.1126/science.1107834

Gjøsaeter, J. and Kawaguchi, K. 1980. A review of the world resources of mesopelagic fish. *FAO Fisheries Technical Paper*, *193*(193).

Herbert, G., Kermabon, C., Grelet, J. and Bourles, B. 2015. French PIRATA cruises S-ADCP data processing. *Mercator Ocean - Quaterly Newsletter*, (52), 22–26. Accessed: https://archimer.ifremer.fr/doc/00272/38320/

Huang, N. E. and Shen, S. S. P. 2014. *Hilbert-Huang Transform and Its Applications*. *Interdisciplinary Mathematical Sciences* (2ª, Vol. 5). Singapore: World Scientific, 1–26 pp. DOI: https://doi.org/doi:10.1142/5862

Hummels, R., Brandt, P., Dengler, M., Fischer, J., Araujo, M., Veleda, D. and Durgadoo, J. V. 2015. Interannual to decadal changes in the western boundary circulation in the Atlantic at 11°S. *Geophysical Research Letters*, *42*(18), 7615–7622. DOI: https://doi.org/10.1002/2015GL065254

Huthnance, J. M. 1973. Tidal current asymmetries over the Norfolk Sandbanks. *Estuarine and Coastal Marine Science*, *1*(1), 89–99. DOI: https://doi.org/10.1016/0302-3524(73)90061-3

Huthnance, J. M. 1995. Circulation, exchange and water masses at the ocean margin: the role of physical processes at the shelf edge. *Progress in Oceanography*, *35*(4), 353–431. DOI: https://doi.org/10.1016/0079-6611(95)80003-C

Kbaier Ben Ismail, D., Lazure, P. and Puillat, I. 2016. Application of Hilbert-Huang decomposition to temperature and currents data in the Réunion island. *OCEANS 2016 MTS/IEEE Monterey* (pp. 1–9). IEEE. DOI: https://doi.org/10.1109/OCEANS.2016.7761460

Kelly, J. T. and Klimley, A. P. 2012. Relating the swimming movements of green sturgeon to the movement of water currents. *Environmental Biology of Fishes*, *93*(2), 151–167. DOI: https://doi.org/10.1007/s10641-011-9898-8

Klevjer, T. A., Irigoien, X., Røstad, A., Fraile-Nuez, E., Benítez-Barrios, V. M. and Kaartvedt., S. 2016. Large scale patterns in vertical distribution and behaviour of mesopelagic scattering layers. Scientific Reports, 6(1), 19873. DOI: https://doi.org/10.1038/srep19873

Lamb, K. G. 2014. Internal Wave Breaking and Dissipation Mechanisms on the Continental Slope/Shelf. *Annual Review of Fluid Mechanics*, *46*(1), 231–254. DOI: https://doi.org/10.1146/annurev-fluid-011212-140701

Langbehn, T., Aksnes, D., Kaartvedt, S., Fiksen, Ø. and Jørgensen, C. 2019. Light comfort zone in a mesopelagic fish emerges from adaptive behaviour along a latitudinal gradient. *Marine Ecology Progress Series*, *623*, 161–174. DOI: https://doi.org/10.3354/meps13024

Lentz, S. J. 2001. The influence of stratification on the wind-driven cross-shelf circulation over the North Carolina shelf. *Journal of Physical Oceanography*, *31*(9), 2749–2760. DOI: https://doi.org/10.1175/1520-0485(2001)031<2749:TIOSOT>2.0.CO;2

Lentz, S. J. and Chapman, D. C. 2004. The importance of nonlinear cross-shelf momentum flux during wind-driven coastal upwelling. *Journal of Physical Oceanography*, *34*(11), 2444–2457. DOI: https://doi.org/10.1175/JPO2644.1

Lévy, M., Franks, P. J. S. and Smith, K. S. 2018. The role of submesoscale currents in structuring marine ecosystems. *Nature Communications*, *9*(1), 4758. DOI: https://doi.org/10.1038/s41467-018-07059-3

Loder, J. W. 1980. Topographic Rectification of Tidal Currents on the Sides of Georges Bank. *Journal of Physical*

Oceanography, *10*(9), 1399–1416. DOI: https://doi.org/10.1175/1520-0485(1980)010<1399:TROTCO>2.0.CO;2

Loder, J. W. and Wright, D. G. 1985. Tidal rectification and frontal circulation on the sides of Georges Bank. *Journal of Marine Research*, *43*(3), 581–604. DOI: https://doi.org/10.1357/002224085788440367

Macedo, S. J., Flores Montes, M. de J., Costa, K. M. P. 2009. Condições hidrológicas na zona econômica exclusiva do Nordeste do Brasil. In: *HAZIN, FHV. Meteorologia e Sensoriamento Remoto, Oceanografia Física, Oceanografia Química e Oceanografia Geológica*. *Programa REVIZEE – Score Nordeste*. Fortaleza, Ed. Martins and Cordeiro, vol. 1, 104-134.

Matano, R. P. and Palma, E. D. 2008. On the Upwelling of Downwelling Currents. *Journal of Physical Oceanography*, *38*(11), 2482–2500. DOI: https://doi.org/10.1175/2008JPO3783.1

Nagai, T., Hasegawa, D., Tanaka, T., Nakamura, H., Tsutsumi, E., Inoue, R. and Yamashiro, T. 2017. First Evidence of Coherent Bands of Strong Turbulent Layers Associated with High-Wavenumber Internal-Wave Shear in the Upstream Kuroshio. *Scientific Reports*, *7*(1), 14555. DOI: https://doi.org/10.1038/s41598-017-15167-1

Neilson, J. D. and Perry, R. I. 1990. Diel Vertical Migrations of Marine Fishes: an Obligate or Facultative Process? *Advances in Marine Biology* (Vol. 26, pp. 115–168). Academic Press. DOI: https://doi.org/10.1016/S0065-2881(08)60200-X

O'Dor, R. K., Adamo, S., Aitken, J. P., Andrade, Y., Finn, J., Hanlon, R. T. and Jackson, G. D. 2002. Currents as environmental constraints on the behavior, energetics and distribution of squid and cuttlefish. *Bulletin of Marine Science*, *71*(2), 601–617. Accessed: https://www.ingentaconnect.com/content/umrsmas/bullmar/2002/00000071/00000002/art00004

Oke, P. R. and Middleton, J. H. 2000. Topographically Induced Upwelling off Eastern Australia. *Journal of Physical Oceanography*, *30*(3), 512–531. DOI: https://doi.org/10.1175/1520-0485(2000)030<0512:TIUOEA>2.0.CO;2

Pineda, J. 1994. Internal tidal bores in the nearshore: warm-water fronts, seaward gravity currents and the onshore transport of neustonic larvae. *Journal of Marine Research*, *52*(3), 427–458. DOI: https://doi.org/10.1357/0022240943077046

Pingree, R. D., Mardell, G. T. and Cartwright, D. E. 1981. Slope Turbulence, Internal Waves and Phytoplankton Growth at the Celtic Sea Shelf-Break [and Discussion]. *Philosophical Transactions of the Royal Society A: Mathematical, Physical and Engineering Sciences*, *302*(1472), 663–682. DOI: https://doi.org/10.1098/rsta.1981.0191

Quilfen, Y. & Chapron, B. 2019. Ocean Surface Wave-Current Signatures From Satellite Altimeter Measurements. *Geophysical Research Letters*, *46*(1), 253–261. DOI: https://doi.org/10.1029/2018GL081029

Quilfen, Y. & Chapron, B. 2021. On denoising satellite altimeter measurements for high-resolution geophysical signal analysis. *Advances in Space Research*, *68*(2), 875–891. DOI: https://doi.org/10.1016/j.asr.2020.01.005

Robinson, I. S. 1981. Tidal vorticity and residual circulation. *Deep Sea Research Part A, Oceanographic Research Papers*, *28*(3), 195–212. DOI: https://doi.org/10.1016/0198-0149(81)90062-5

Rochford, D. 1991. 'Upwelling': Does it need a stricter Definition? *Marine and Freshwater Research*, *42*(1), 45. DOI: https://doi.org/10.1071/MF9910045

Romero-Romero, S., Choy, C. A., Hannides, C. C. S., Popp, B. N. and Drazen, J. C. 2019. Differences in the trophic ecology of micronekton driven by diel vertical migration. *Limnology and Oceanography*, *64*(4),

1473–1483. DOI: https://doi.org/10.1002/lno.11128

Roughan, M. and Middleton, J. H. 2002. A comparison of observed upwelling mechanisms off the east coast of Australia. *Continental Shelf Research*, *22*(17), 2551–2572. DOI: https://doi.org/10.1016/S0278-4343(02)00101-2

Salvetat, J., Bez, N., Habasque, J., Lebourges-Dhaussy, A., Lopes, C., Roudaut, G., Simier, M., Travassos, P., Vargas, G. and Bertrand, A. 2022. Comprehensive spatial distribution of tropical fish assemblages from multifrequency acoustics and video fulfils the island mass effect framework. *Scientific Reports*, *12*(1). DOI: https://doi.org/10.1038/s41598-022-12409-9

Sato, M. and Benoit-Bird, K. J. 2024. Diel Vertical Migrators Respond to Short-Term Upwelling Events. *Geophysical Research Letters*, *51*(2), 1–11. DOI: https://doi.org/10.1029/2023GL105387

Schaeffer, A., Roughan, M. and Morris, B. D. 2013. Cross-Shelf Dynamics in a Western Boundary Current Regime: Implications for Upwelling. *Journal of Physical Oceanography*, *43*(5), 1042–1059. DOI: https://doi.org/10.1175/jpo-d-12-0177.1

Schott, F. A., Brandt, P., Hamann, M., Fischer, J. and Stramma, L. 2002. On the boundary flow off Brazil at 5–10°S and its connection to the interior tropical Atlantic. *Geophysical Research Letters*, *29*(17), 21-1-21–4. DOI: https://doi.org/10.1029/2002GL014786

Schott, F. A., Dengler, M., Zantopp, R., Stramma, L., Fischer, J. and Brandt, P. 2005. The Shallow and Deep Western Boundary Circulation of the South Atlantic at 5°–11°S. *Journal of Physical Oceanography*, *35*(11), 2031–2053. DOI: https://doi.org/10.1175/JPO2813.1

Silva, M. V. B., Ferreira, B., Maida, M., Queiroz, S., Silva, M., Varona, H. L., Araújo, T. C. M. and Araújo, M. 2022. Flow-topography interactions in the western tropical Atlantic boundary off Northeast Brazil. *Journal of Marine Systems*, *227*, 103690. DOI: https://doi.org/10.1016/j.jmarsys.2021.103690

Silva, M., Araújo, M., Servain, J. and Pierrick, P. 2009a. Circulation and heat budget in a regional climatological simulation of the Southwestern Tropical Atlantic. *Tropical Oceanography*, *37*(1–2). DOI: https://doi.org/10.5914/tropocean.v37i1-2.5156

Silva, M., Araujo, M., Servain, J., Penven, P. and Lentini, C. A. D. A. 2009b. High-resolution regional ocean dynamics simulation in the southwestern tropical Atlantic. *Ocean Modelling*, *30*(4), 256–269. DOI: https://doi.org/10.1016/j.ocemod.2009.07.002

Song, H., Bai, Y., Pinheiro, L., Dong, C., Huang, X. & Liu, B. 2012. Analysis of ocean internal waves imaged by multichannel reflection seismics, using ensemble empirical mode decomposition. *Journal of Geophysics and Engineering*, *9*(3), 302–311. DOI: https://doi.org/10.1088/1742-2132/9/3/302

Stern, M. E. and Shen, C. Y. 1975. *Displacement and rectification of planetary fluids*. *Geophysical Fluid Dynamics* (Vol. 7). 81–118 pp. DOI: https://doi.org/10.1080/03091927508242614

Stramma, L., Fischer, J. and Reppin, J. 1995. The North Brazil Undercurrent. *Deep Sea Research Part I: Oceanographic Research Papers*, *42*(5), 773–795. DOI: https://doi.org/10.1016/0967-0637(95)00014-W

Sutton, T. T. 2013. Vertical ecology of the pelagic ocean: classical patterns and new perspectives. *Journal of Fish Biology*, *83*(6), 1508–1527. DOI: https://doi.org/10.1111/jfb.12263

Sutton, T. T. and Hopkins, T. L. 1996. Trophic ecology of the stomiid (Pisces: Stomiidae) fish assemblage of the eastern Gulf of Mexico: Strategies, selectivity and impact of a top mesopelagic predator group. *Marine Biology*, *127*(2), 179–192. DOI: https://doi.org/10.1007/BF00942102

Thévenin, M. R., Pereira, J. and Lessa, G. C. 2019. Shelf-break upwelling on a very narrow continental shelf adjacent to a western boundary current formation zone. *Journal of Marine Systems*, *194*(October

2018), 52–65. DOI: https://doi.org/10.1016/j.jmarsys.2019.02.008

Todd, R. E., Chavez, F. P., Clayton, S., Cravatte, S. E., Goes, M. P., Graco, M. I., Lin, X., Sprintall, J., Zilberman, N. V., … Zhang, L. 2019. Global perspectives on observing ocean boundary current systems. *Frontiers in Marine Science*, *6*(JUL), 423. DOI: https://doi.org/10.3389/fmars.2019.00423

Veleda, D. D., Araujo, M., Silva, M., MONTAGNE, R., ARAÚJO, R., Araújo, M., Silva, M. and MONTAGNE, R. 2011. Seasonal and interannual variability of the southern south Equatorial Current bifurcation and meridional transport along the eastern brazilian edge. *Tropical Oceanography*, *39*(1), 27–59. DOI: https://doi.org/10.5914/to.2011.0051

Weigert, S. C. and Madureira, L. S. P. 2011. Registros acústicos biológicos detectados na Zona Econômica Exclusiva da região Nordeste do Brasil - Uma classificação em ecotipos funcionais. *Atlântica*, *33*(1), 15–32. DOI: https://doi.org/10.5088/atl. 2011.33.1.15

Wu, L., Cai, W., Zhang, L., Nakamura, H., Timmermann, A., Joyce, T., McPhaden, M. J., Alexander, M., Qiu, B., Visbeck, M., Chang, P. and Giese, B. 2012. Enhanced warming over the global subtropical western boundary currents. *Nature Climate Change*, *2*(3), 161–166. DOI: https://doi.org/10.1038/nclimate1353

Wu, Z. and Huang, N. E. 2009. Ensemble Empirical Mode Decomposition: A Noise-Assisted Data Analysis Method. *Advances in Adaptive Data Analysis*, *01*(01), 1–41. DOI: https://doi.org/10.1142/S1793536909000047

Yanagi, T. 1987. Classification of 'siome', streaks and fronts. *Journal of the Oceanographical Society of Japan*, *43*(3), 149–158. DOI: https://doi.org/10.1007/BF02109215

Yancey, P. H., Lawrence-Berrey, R. and Douglas, M. D. 1989. Adaptations in mesopelagic fishes. *Marine Biology*, *103*(4), 453–459. DOI: https://doi.org/10.1007/BF00399577

Zaron, E. D. & Elipot, S. 2021. An assessment of global ocean barotropic tide models using geodetic mission altimetry and surface drifters. *Journal of Physical Oceanography*, *51*(1), 63–82. DOI: https://doi.org/10.1175/JPO-D-20-0089.1

Zembruscki, S. G., Barreto, H. T., Palma, J. C. and Milliman, J. D. 1972. Estudo preliminar das províncias geomorfológicas da margem continental brasileira. *Congresso Brasileiro de Geologia* (Vol. 26, pp. 187–209). Accessed: https://www.sbgeo.org.br/assets/admin/imgCk/files/Anais/ANAIS_DO_XXVI CBG_1972_V2.pdf

This preprint was submitted under the following conditions:

- The authors declare that the necessary Terms of Free and Informed Consent of participants or patients in the research were obtained and are described in the manuscript, when applicable.
- The authors declare that the preparation of the manuscript followed the ethical norms of scientific communication.
- The authors declare that they are aware that they are solely responsible for the content of the preprint and that the deposit in SciELO Preprints does not mean any commitment on the part of SciELO, except its preservation and dissemination.
- The authors declare that the data, applications, and other content underlying the manuscript are referenced.
- The deposited manuscript is in PDF format.
- The authors declare that the research that originated the manuscript followed good ethical practices and that the necessary approvals from research ethics committees, when applicable, are described in the manuscript.
- The authors declare that once a manuscript is posted on the SciELO Preprints server, it can only be taken down on request to the SciELO Preprints server Editorial Secretariat, who will post a retraction notice in its place.
- The authors agree that the approved manuscript will be made available under a Creative Commons CC-BY license.
- The submitting author declares that the contributions of all authors and conflict of interest statement are included explicitly and in specific sections of the manuscript.
- The authors declare that the manuscript was not deposited and/or previously made available on another preprint server or published by a journal.
- If the manuscript is being reviewed or being prepared for publishing but not yet published by a journal, the authors declare that they have received authorization from the journal to make this deposit.
- The submitting author declares that all authors of the manuscript agree with the submission to SciELO Preprints.